What is the Radiation Impact of Extreme Solar Energetic Particle Events on Mars?

Jian Zhang[1], Jingnan Guo[1,2], Mikhail I. Dobynde[1]

[1]Deep Space Exploration Laboratory/School of Earth and Space Sciences, University of Science and Technology of China, Hefei, PR China
[2]CAS Center for Excellence in Comparative Planetology, USTC, Hefei, PR China

Key Points:

- We calculate dose, dose equivalent, and effective dose induced by extreme Solar Energetic Particle Events on and below the martian surface
- Surface pressure which is related to geographic altitude significantly affects the surface radiation level
- We can predict the surface pressure-dependent SEP-induced radiation solely based on the SEP flux at the pivot energies.

Corresponding author: Jingnan Guo, jnguo@ustc.edu.cn

Abstract

Solar Energetic Particles (SEP) are one of the major sources of the martian radiation environment. It is important to understand the SEP-induced martian radiation environment for future human habitats on Mars. Due to the lack of global intrinsic magnetic field, SEPs can directly propagate through and interact with its atmosphere before reaching the surface and subsurface of Mars. Since Mars has many high mountains and low-altitude craters where the atmospheric thickness can be more than 10 times different from one another, the SEP-resulted surface radiation level may be very different from one location to another. We thus consider the influence of the atmospheric depths on the martian radiation levels including the absorbed dose, dose equivalent, and (human-)body effective dose induced by SEPs at varying heights above and below the martian surface. The state-of-the-art Atmospheric Radiation Interaction Simulator based on GEometry And Tracking Monte-Carlo method (AtRIS/GEANT4) has been employed for simulating particle interactions with the martian atmosphere and terrain. We find that even the thinnest martian atmosphere reduces radiation dose from that in deep space by at least 65%, and the shielding effect increases for denser atmosphere. Furthermore, we present a method to quickly forecast the SEP-induced radiation in different regions of Mars with different surface pressures.

Plain Language Summary

On Earth, the global magnetic field and dense atmosphere can efficiently protect us from the radiation risk induced by Solar Energetic Particles (SEP). On Mars, however, we are not so lucky. The lack of effective magnetic field and a thin atmosphere make Mars much more exposed to space radiation. It is therefore necessary to study the radiation impact on future humans exploring Mars. In this paper, we study the radiation level induced by SEPs at different locations on Mars and find that the martian atmosphere, even with the thinnest condition on top of Mount Olympus, can reduce at least 65% of the radiation dose. In support of mitigating radiation risks for future Mars missions, we find statistical correlations of the SEP radiation level on Mars with the SEP properties and derive convenient prediction functions which relate the SEP fluence at a certain energy with the martian surface dose.

1 Introduction

As flying to Mars is becoming extremely compelling for space agencies and the general public, it is important to consider all potential risks for astronauts, which may encounter during such a mission. One of the serious hazards is induced by space radiation which exists both during interplanetary flight and on the surface of Mars (e.g., Cucinotta et al., 2013; Zeitlin et al., 2013; Hassler et al., 2014; Guo et al., 2021). Radiation environment in space mainly consists of Galactic Cosmic Rays (GCRs) and Solar Energetic Particles (SEPs). GCRs are omnipresent low-intensity background flux of high-energy (up to TeV/nucleon) fully ionized elements from hydrogen to nickel and beyond. In contrast, SEPs are mostly protons from solar eruptions accelerated up to several GeV. SEPs can cause very significant radiation flux enhancements within a short time period. When referring to extreme SEPs and their space weather impact on Earth, the Ground Level Enhancement (GLE) events are of particular interest. They are often accelerated by large solar eruptions and contain protons with energies above a few hundreds of MeV and even up to a few GeVs. Consequently, as its name suggests, GLE particles may be able to penetrate the Earth's magnetic field and atmosphere to cause enhancements detected by particle detectors, such as muon or neutron monitors, on the Earth's surface (e.g., Miroshnichenko et al., 2013). During large SEPs, the CME-shock may have the strength to keep accelerating particles in the interplanetary space as they propagate outward and another

SEP component called the Energetic Storm Particles (ESP) is often observed upon the arrival of the shock at an observer (Bryant et al., 1962).

Before reaching the martian surface, energetic particles interact with the atmosphere. However, Mars' surface pressure is only about one percent of that on Earth and it can vary by more than one order of magnitude due to the martian topography, e.g. 82 Pa on Mount Olympus and 1200 Pa within the Greek plain. While propagating through the martian atmosphere, energetic particles lose their energy and generate secondaries via nuclear interactions (such as neutrons, electrons, gammas, muons, etc.) which increase the radiation level. The interaction of GCRs with the martian atmosphere of different thicknesses has been recently studied (Saganti et al., 2004; Ehresmann et al., 2011; Guo et al., 2017; Zhang et al., 2022). It has been found that GCR-induced surface radiation level (quantified as dose rate) does not differ significantly, within about 10%, between different pressure conditions as suggested both by observations by the Radiation Assessment Detector (RAD, Hassler et al., 2012) at Gale Crater (Guo et al., 2017) and by detailed modeling results (Zhang et al., 2022). In comparison with GCRs, SEPs cover a lower energy range and are more likely to stop or lose energy in the atmosphere, suggesting that they are more susceptible to the thickness of the martian atmosphere. For example, the martian atmosphere at Gale Crater with a surface atmospheric pressure of about 830 Pa, corresponding to column density of 22.5 g/cm^2 can stop protons below the energy of about 160 MeV from reaching the surface(Guo, Banjac, et al., 2019). Thus, the variation of SEP-induced radiation level should be greater than GCR's at different locations on Mars where the surface atmospheric column density varies significantly, e.g., 2.23 and 32.2 g/cm^2 for Mount Olympus and Greek plain, respectively. RAD is the only radiation detector on Mars and can not simultaneously measure the surface SEP radiation level under two different pressures. Previous modeling studies mainly focused on the "global radiation map" of Mars induced by GCRs (e.g., Saganti et al., 2004; Da Pieve et al., 2021). while how this map may change under extreme SEP events still remain unclear. Therefore, we here investigate the impact of extreme SEP Events (i.e., GLE events) on the surface radiation environment in a few representative regions on Mars with surface pressures varying significantly from one another.

With this purpose, we apply a GEometry And Tracking (GEANT4, Agostinelli et al., 2003) based particle transport code named Atmospheric Radiation Interaction Simulator (AtRIS, Banjac et al., 2018), which is a state-of-the-art modeling tool developed to simulate the propagation of energetic particles through planetary atmosphere and regolith. AtRIS has been previously applied to study the martian radiation environment with a focus on GCRs and validated against the RAD measurements (Guo, Banjac, et al., 2019; Röstel et al., 2020; Zhang et al., 2022). Here it is used to study the SEP-induced surface radiation environment at different Mars' locations with vastly different atmospheric depths. The article is organized as following: Section 2 introduces and describes the methodology, model setup and input parameters for the study; Section 3 shows and discusses the results and Section 4 summarizes the main results and concludes our study.

2 Methods

2.1 GLE Spectra

There is few study on retrieving the spectra of SEPs arriving at Mars due to the lack of observational data, while the method of studying the SEP spectra at Earth based on both ground-based and space-borne observations is already very sophisticated. Tylka and Dietrich (2009) analyzed the time-integrated fluence spectra of GLE events based on combined spacecraft and neutron monitor measurements and found that the fluence spectra in rigidity can be represented with a double power law function known as the Band function (Band et al., 1993). With this method, Raukunen et al. (2018, Table2) calibrated spectral parameters for 59 GLE events together with the ESP components of

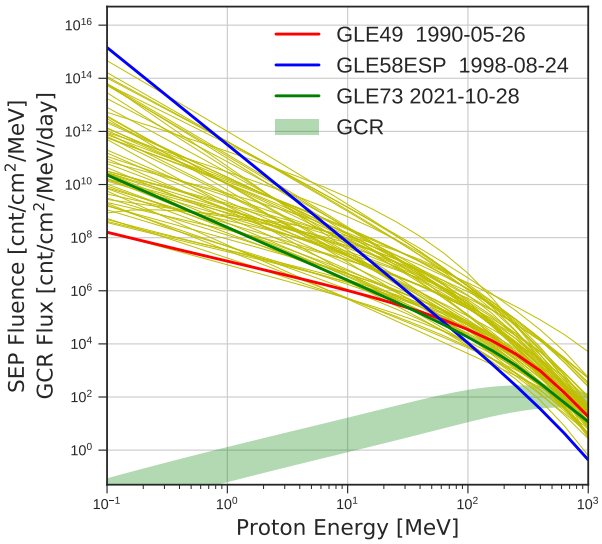

Figure 1. The time-integrated fluence spectra of 67 GLE events are represented by colored lines. Three events are marked by different colors. The green shadow represents the GCR flux derived from the Badhwar O'Neil 2014 model (O'Neill et al., 2015) with the solar modulation between 400 MV and 1000 MV.

6 events (GLE42, GLE43, GLE58, GLE59, GLE62, and GLE65) occurring in 1956–2012. In addition, we also include the spectra of the most recent two events: GLE72 (Bruno et al., 2019) and GLE73 (Guo et al., 2023; Martucci et al., 2023). All of the GLE event spectra used in this article are shown in Figure 1. Compared to the daily flux of GCR protons, the fluence of SEPs below 100 MeV is significantly higher: the difference is between 2 and 14 orders of magnitude.

Before applying these spectra to the Mars model, we need to consider the evolution of SEP flux due to the different separation of Mars and Earth from the corresponding original flare/CME site (e.g., Lario et al., 2013). This difference would also vary from one event to another due to the orbital movement of the planets and the "ad-hoc" location of the flare/CME site. Since the longitudinal separation of one observer to the eruption site is arbitrary and thus statistically equivalent for Mars and Earth, we can scale the SEP flux from Earth (at 1 AU) to Mars (at 1.5 AU) only considering the radial gradient of the SEP flux. In this study, we suppose that flux intensity decreases as $\sim 1/r^2$ with the distance from the Sun thus a scaling factor $1/1.5^2 = 0.44$ should be applied to multiply the SEP fluence at Earth to convert it into that at Mars.

2.2 Mars Radiation Model

In the Mars model, the atmospheric properties including the composition ($\sim 95\%$ CO_2), density, temperature and their variation over altitude are defined by the Mars Climate Database (MCD, Forget et al., 1999, http://www-mars.lmd.jussieu.fr). It is a database of meteorological fields derived from General Circulation Model (GCM) numerical simulations of the martian atmosphere and validated using available observational data. Guo, Banjac, et al. (2019), Röstel et al. (2020) and Zhang et al. (2022) have implemented MCD in AtRIS (explained later in detail) to model the Mars radiation environment, and Zhang et al. (2022) set up 6 respective models under 6 martian surface pressures of 82, 305, 529,

753, 975, and 1200 Pa to assess the variation of the GCR radiation levels at different martian locations. In this work, we further investigate the influence of atmospheric thickness on the SEP radiation with the same model used in Zhang et al. (2022).

The martian soil is defined as a substance with a density of 1.79 g/cm^2 and composed of 50% Si, 40% O, and 10% Fe which is close to the Andesite Rock (AR) scenario considered by Röstel et al. (2020, AR mass fraction is 44% O, 27% Si, 12% Fe). The model provides particle spectra at 80 altitudes distributed in a logarithmic scale from the surface up to 80 km and at 40 evenly-distributed depth layers in the martian soil down to 10 m.

Atmospheric Response Matrices (ARMs) makes AtRIS a convenient tool (Banjac et al., 2018) to save simulation time and they are obtained by simulating primary particles through the atmospheric model for different primary-secondary case (e.g., protons producing neutrons) and directions (upwards & downwards). In the first run, the average ionization and interaction process of a particle with specific energy penetrating the atmosphere is simulated, and the histogram of secondary particles caused by primary particles with different energy bins are listed in columns of an ARM. In the following calculations, secondary particle spectra can be obtained simply by multiplying the incoming GCR/SEP spectrum with the ARM at a certain output layer, rather than running a new simulation with a new spectrum with the math description detailed in Guo, Banjac, et al. (2019).

With the output particle spectra at a certain layer of our martian radiation model, we can then obtain the absorbed dose, dose equivalent (ICRP, 2013) and effective dose (ICRP, 2007) using the energy and particle-dependent dose conversion factors, as described in detail by Dobynde et al. (2021) and Zhang et al. (2022, section 2.3). The absorbed dose (expressed in the unit of J kg^{-1}, or Gray, or Gy) is defined as the total energy deposited by particles per unit of material mass. It is a key parameter that is directly measurable for evaluating the radiation effect of high-energy particles when they interact with the target. In this study, we will calculate the absorbed dose in two phantoms: a 300-μm-thick silicon slab representing the silicon dosimeter of RAD, and a 15-cm radius water sphere that approximates a human torso. The latter phantom is also applied to calculate the dose equivalent and effective dose since we can not directly characterize the biological effect of particle radiation on the human body from the absorbed dose. The biological damage in tissue depends on the linear energy transfer (LET) which is the energy dE deposited along a path length of dx. By multiplying the absorbed dose by LET-dependent quality factor Q(LET) (ICRP, 1992), we can obtain the dose equivalent. Further, the radiation damage to the entire human body is characterized by the effective dose as a sum of tissue-weighted dose equivalent values in 15 critical organs (ICRP, 2007). Here we use mean shielding values of a particular organ to identify the dose equivalent at this corresponding spherical layer as described by Matthiä et al. (2013). Finally, for the given 67 spectra of GLE events, the absorbed dose, dose equivalent and effective dose above and below the martian surface can be calculated for each of the 6 selected locations. The results are presented and discussed in the following section.

3 Results and Discussion

With the simulation methods introduced in section 2 and for each GLE event, we can obtain the particle spectra (of both primary particles and their secondary particles) and corresponding radiation level generated at each of the 6 locations through different depths of the atmosphere and regolith. GLE73 which took place on 2021 October 28 is the most recent GLE event and has been studied in detail combining observations from both Earth and Mars (Guo et al., 2023). So we also employ GLE73 as an example to show its radiation impact throughout the martian atmosphere under different surface atmospheric pressures.

3.1 Radiation environment induced by GLE73

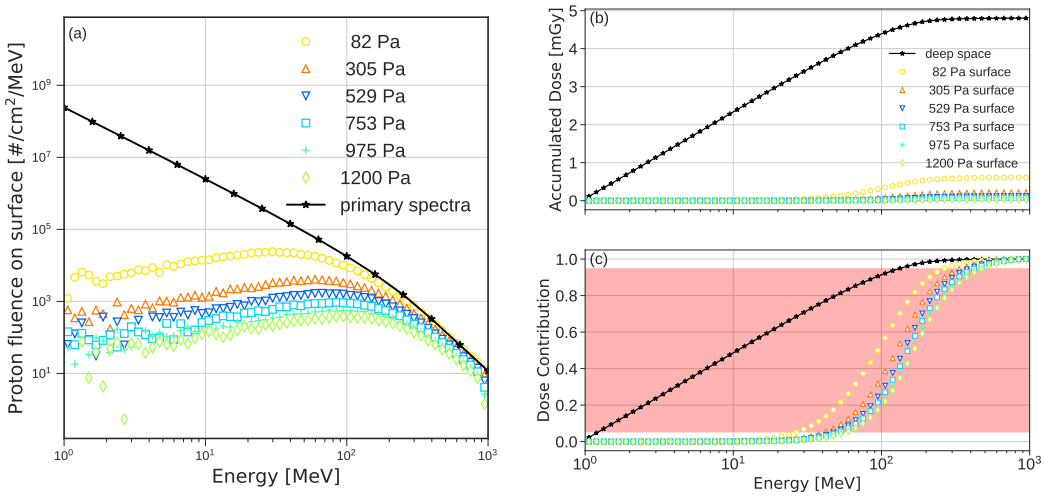

Figure 2. (a): The input primary spectra of GLE73 (2021-10-28, black star line) scaled to the distance of Mars (and integrated over 2π) and the output proton fluence at the martian surface under the scenarios of surface pressure for 82, 305, 529, 753, 975 and 1200 Pa (shown in different colors). (b): The accumulated absorbed dose (in a 15-cm radius water sphere) of protons (y-axis, in units of mGy) lower than certain energy (x-axis) for different cases: 2π-deep space (black star line) and under different pressures on the surface of Mars (colored lines). (c): The same as in (b) but with the accumulation scaled to the maximum value of each case.

Figure 2(a) compares the primary proton spectra of GLE73 (integrated over a solid angle of 2π considering a planetary surface without atmospheric shielding) with the output proton spectra on the martian surface under different surface pressures. The shielding effect of the martian atmosphere is clearly shown for protons with energy below 100 MeV and is more significant with increasing surface atmospheric pressure. Even when the surface pressure is only 82 Pa (the case of Mount Olympus), the output surface spectrum of protons has a considerable reduction below $\sim$ 150 MeV and is more than four orders of magnitude smaller than the primary spectrum at 1 MeV. While under the surface atmospheric pressure of 1200 Pa, the output surface proton fluence has decreased further: at 100 MeV, it reduced by over one order of magnitude compared to the deep-space spectra and the 82-Pa spectra. At energy lower than 10 MeV, the difference of the surface proton fluence under different surface pressures has reached about two orders of magnitude.

The absorbed dose on the surface of Mars is mainly contributed by protons in case of large SEP events. As shown in Figure 2(b), the energy-accumulated absorbed dose of protons, which is calculated in the 15-cm-radius water sphere phantom placed in deep space, steadily increases to 4.4 mGy at 100 MeV, then slowly reaches a plateau of 4.8 mGy. In comparison, the surface dose under 82 Pa is only about 0.6 mGy meaning that the martian atmosphere of only about 2.23 g/cm^2 can reduce about 88% of the total radiation dose induced by GLE protons in deep space.The surface dose is significantly lower for other pressures that can shield more than 98% of the deep-space dose, e.g., it is 0.08 mGy under 753 Pa. Figure 2(c) shows that the energy interval dominating 90% of the proton-induced radiation is 1 - 135 MeV in deep space and shifts to 25 - 270 MeV for the 82-Pa case, and then shifts further to 55 - 485 MeV for the 1200-Pa case.

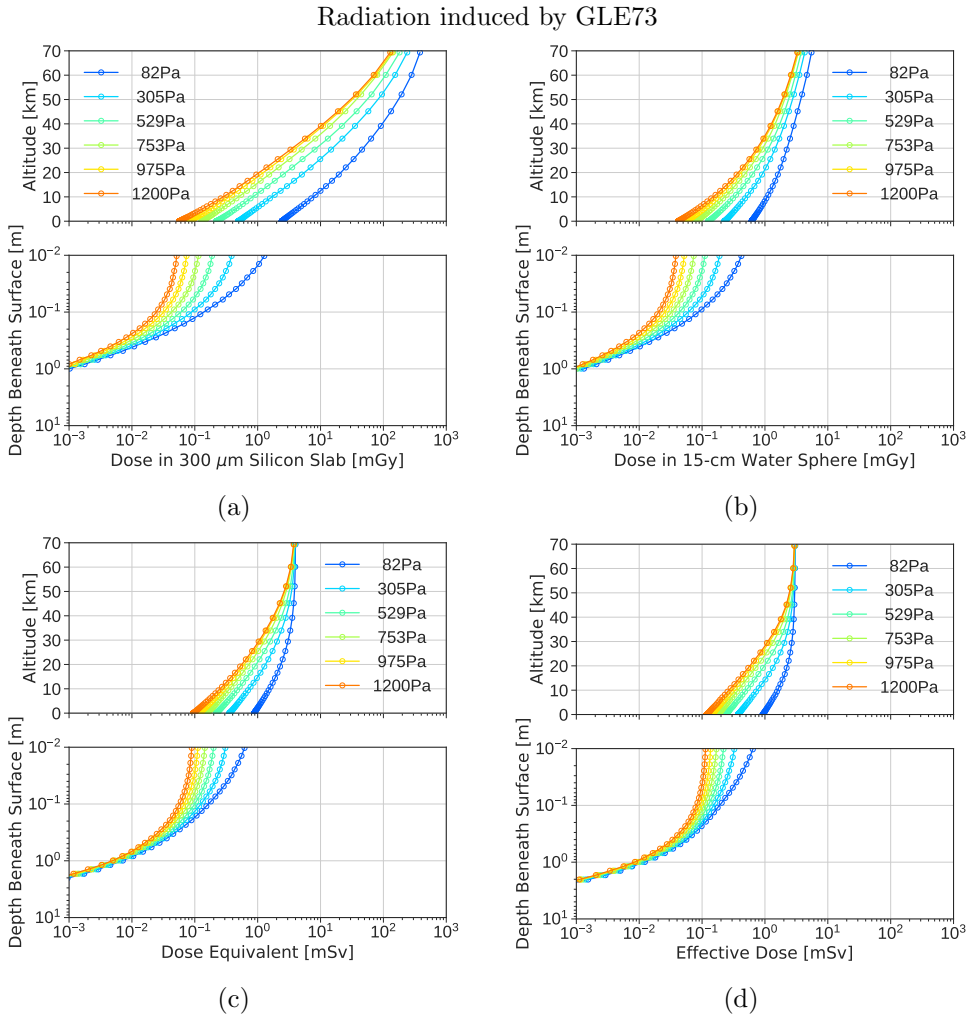

Figure 3. Absorbed dose (in units of mGy) in a 300-μm-thick silicon slab (panel a) and in a 15-cm radius water sphere (panel b) at various locations on Mars with surface pressures of 82, 305, 529, 753, 975, 1200 Pa from 70-km atmospheric height to the surface and down to 10 m below the surface. (c) and (d) panels show the dose equivalent and effective dose calculated based on a 15-cm-radius water sphere phantom, respectively.

Figure 3(a) and (b) show the absorbed dose induced by primary GLE73 protons calculated based on the silicon slab phantom and on the water sphere phantom, respectively. The results are shown from 70-km atmospheric height to the surface and down to several meters below the surface (each line) and at various locations on Mars with surface pressures of 82, 305, 529, 753, 975, 1200 Pa (lines with different colors). Note that secondary particles (e.g, protons, neutrons, electrons, gamma particles, etc) generated by the primary GLE protons in the martian environment that contribute to the absorbed dose are also counted and scored.

The absorbed dose calculated based on the silicon slab phantom quickly decreases from 142 mGy at 70 km altitude to 0.12 mGy on the surface of Mars with an atmospheric pressure of 753 Pa. After the same vertical distance, the absorbed dose of GLE73 is lower under denser atmospheric conditions, and eventually, it becomes negligible (10^{-3} mGy) at around one-meter depth beneath the martian surface. At 70 km, the absorbed dose

in the water sphere (panel b) is over one order of magnitude smaller than that in the silicon slab (panel a) and this difference is mainly caused by low-energy protons which are easily stopped at the outer part of the water sphere. This difference becomes smaller at larger atmospheric depths, e.g., it is only 20% at the 1200-Pa surface, since these low-energy particles are more effectively shielded by the atmosphere.

We also calculated the dose equivalent and effective dose induced by the GLE73 event as shown in Figure 3(c) and (d) respectively. The results of dose equivalent and effective dose are approximately the same. After passing through the martian atmosphere with a surface atmospheric pressure of 1200 Pa, GLE73 causes about 0.1 mSv of effective dose on the surface of Mars, which is around 3% of that in deep space, and approximately one-tenth of that on the surface with an atmospheric pressure of 82 Pa.

3.2 The dependence of the atmospheric shielding on SEP spectral properties

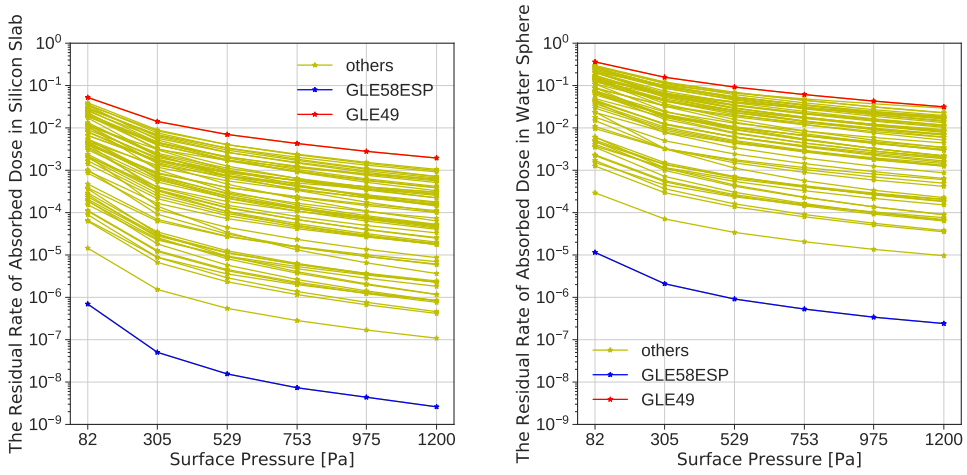

(a) (b)

Figure 4. (a): The ratio of the surface dose to the deep-space dose, i.e., the residual rate $R_{surf/ds}$,(y-axis) calculated in a 300-μm-thick silicon slab for different surface pressures (x-axis) for all the 67 GLE spectra. (b): The residual rate $R_{surf/ds}$ for the absorbed dose calculated based on a water sphere phantom with a radius of 15 cm. The GLE event with the largest $R_{surf/ds}$ is represented in red while that with the smallest $R_{surf/ds}$ is shown in blue, and the remaining 65 GLE events are represented in yellow.

The shielding capability of the martian atmosphere of SEP-induced radiation is related to the atmospheric depth and the SEP spectral properties (such as the relative contribution of low and high energy particles to the total flux). We characterize the shielding capability of the martian atmosphere by defining a residual rate $R_{surf/ds}$, which is the ratio of the surface radiation dose caused by a GLE event to its radiation dose in deep space. Figure 4 compares the residual rates caused by 67 GLE spectra for various surface atmospheric pressures. The residual rate decreases with increasing atmospheric pressure due to a thicker atmosphere stopping more low-energy particles and also slowing down those with higher energies.

Compared to other GLE spectra, the martian atmosphere is the most effective in shielding the radiation caused by GLE58ESP (1998-08-24), with the residual rate for the

absorbed dose in silicon slab ranges from about 8×10^{-7} at the location with surface atmospheric pressure of 82 Pa to approximately 3×10^{-9} at the 1200 Pa location. On the contrary, the residual rate of GLE49 (1990-05-26) is always the highest at all pressure conditions as calculated for the absorbed dose in silicon slab, and it varies from around 5% at 82 Pa to about 0.2% at 1200 Pa. With the identical shielding condition, the residual rate of GLE58ESP is around 5 orders of magnitude lower than that of GLE49 due to the significant contribution of low-energy particles, which are more easily attenuated by the atmosphere. This generally corresponds to a soft power-law spectrum (as shown in Figure 1). In other words, the shielding of the martian atmosphere has a larger influence on primary particles with low energy and consequently the residual rate of GLE event with a harder (or softer) spectrum is larger (or smaller).

When comparing the dose in the water sphere and silicon slab, we also need to pay attention to the low-energy component of the spectra. Generally, low-energy particles contribute more to the dose in the silicon slab than in the water sphere due to the self-shielding effect of the latter with a larger volume and mass. As a result, under the same martian atmospheric condition, the residual rate in the water sphere is higher compared to that in the silicon slab.

3.3 Statistical results and the Pivot energy

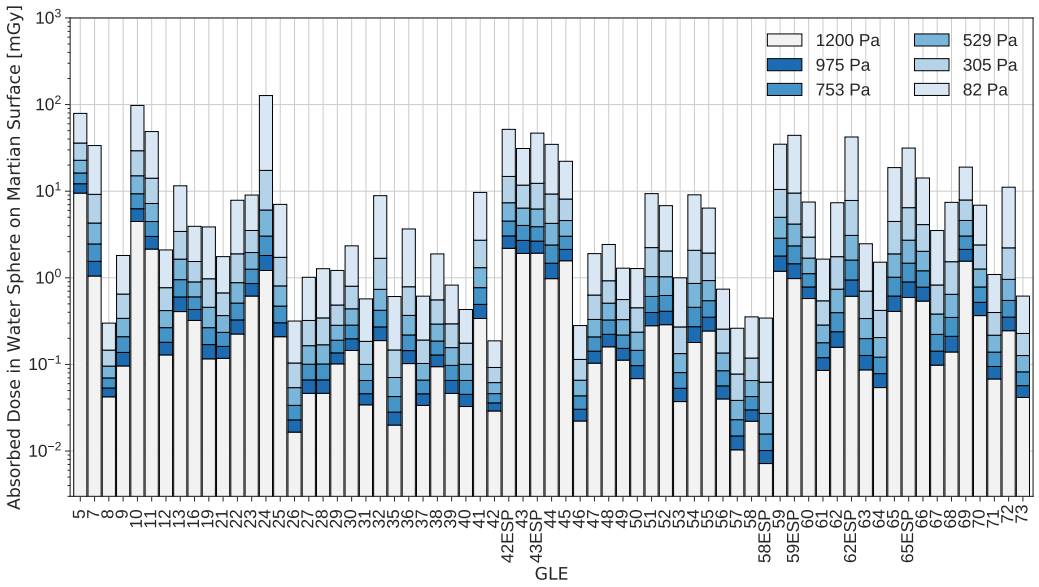

Figure 5. The absorbed dose calculated in a 15-cm-radius water sphere on the martian surface under different surface atmospheric pressures.

As shown in Figure 5, the absorbed dose caused by GLE spectra on the surface of Mars with an atmospheric pressure of e.g., 753 Pa can span three orders of magnitude from about 0.008 mGy for GLE58ESP to more than 10 mGy for GLE5 which approximately equals to a monthly-integrated GCR radiation dose during solar minimum period as measured by RAD during solar cycle 24 (Guo et al., 2021). The maximum dose on Mars shown in the Figure 5 reaches about 100 mGy for GLE24 when the atmospheric pressure is 82 Pa. The pressure dependence of different events is similar for the effective dose as for the absorbed dose which varies from 0.03 mSv to 200 mSv as shown in Figure 6. Thus accounting for pressure dependence of the dose is an important issue for

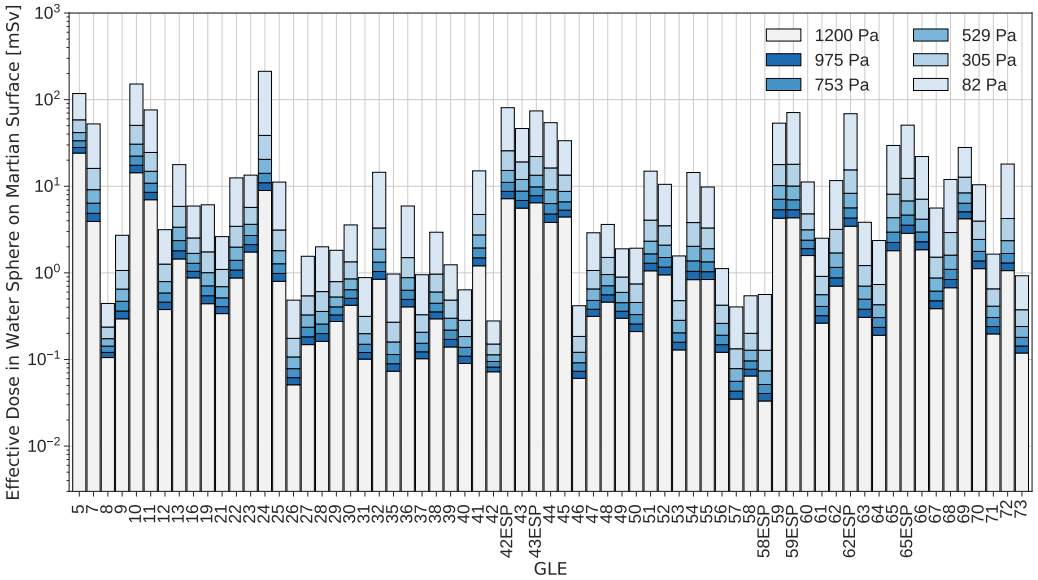

Figure 6. The effective dose calculated based on a 15-cm-radius water sphere phantom on the martian surface under different surface atmospheric pressures.

a quick and accurate forecast of the radiation dose rates caused by different GLEs at various locations on Mars.

Guo, Wimmer-Schweingruber, et al. (2019) statistically studied the effects of different energy ranges, intensities, and power-law index on the SEP-induced radiation on the martian surface. For a given surface pressure of about 840 Pa, they discovered a good correlation between the induced radiation on Mars and the flux of the initial SEP spectra at the so-called pivot energy ($\sim$ 300 MeV). Specifically speaking, the surface dose rate can be directly derived based solely on the SEP flux at this pivot energy while the SEP spectral shape and slope do not affect the surface radiation. Based on the same methodology, we try to correlate the absorbed dose (calculated in the water sphere under different surface pressures) with the original fluence of 67 GLEs at different specific energies to obtain the corresponding pivot energy values and the correlation for determining the surface dose. These values can be used to evaluate the radiation caused by the incoming GLE in different regions with different pressures on the martian surface.

To find the pivot energy for different surface atmospheric pressures, we calculated the Pearson Correlation Coefficient (PCC) of the absorbed and effective dose calculated based on the water sphere phantom induced by each event versus the GLE spectral fluence at different energies. Figure 7(a) plots the PCC versus energy of the original GLE spectra for various cases of pressure. When PCC reaches a maximum value close to 1, the corresponding energy is defined as pivot energy at which the best correlation between the SEP flux and the surface dose can be established. As shown in Figure 7(c), the pivot energy increases from about 110 MeV for 82 Pa to 350 MeV for 1200 Pa because a higher atmosphere column depth corresponds to a higher energy threshold for incoming protons. In Figure 7(b), we show the correlation of the absorbed dose on martian surface versus the primary GLE fluence at the pivot energy (determined in panel (a)). For each of modeled pressure values, we apply a linear function and derive the fitting coefficient between the fluence at the pivot energy and the surface dose based on the following func-

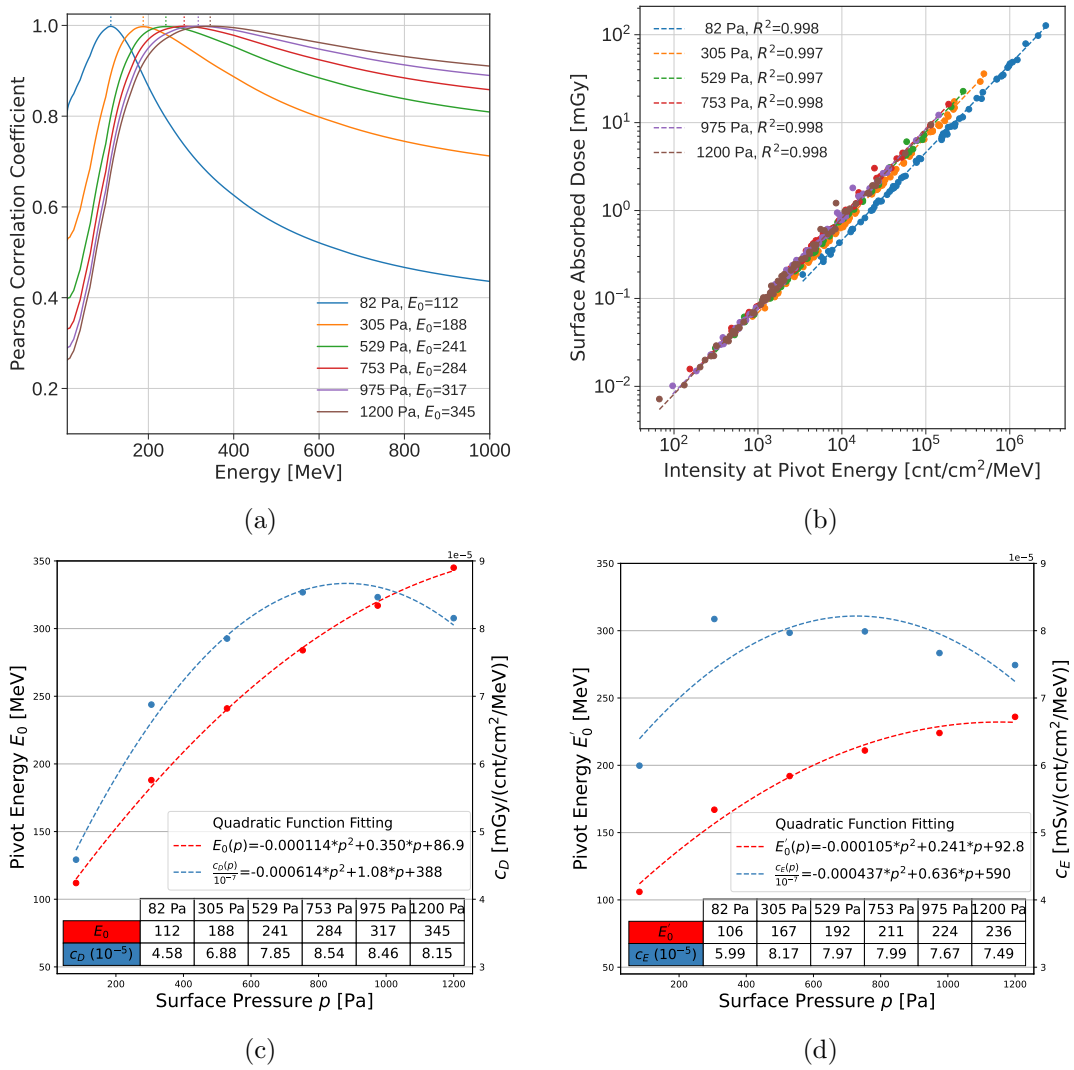

	82 Pa	305 Pa	529 Pa	753 Pa	975 Pa	1200 Pa
E_0	112	188	241	284	317	345
c_D (10^{-5})	4.58	6.88	7.85	8.54	8.46	8.15

	82 Pa	305 Pa	529 Pa	753 Pa	975 Pa	1200 Pa
E_0'	106	167	192	211	224	236
c_E (10^{-5})	5.99	8.17	7.97	7.99	7.67	7.49

Figure 7. (a): The Pearson correlation coefficient between the surface absorbed dose and the intensity at a certain energy for 67 GLE spectra. (b): Colored dots represent the results of 67 GLE spectra, and the colored lines are the corresponding fitting results. (c): The pivot energy $E_0(p)$ and coefficient "$c_D(p)$" (in Equation 1) based on the 6 modeled pressures (dots) and the fitted functions versus the surface atmospheric pressure (dotted lines) for the absorbed dose recorded in the water sphere on the martian surface. (d): The pivot energy $E_0'(p)$ and coefficient "c_E" (in Equation 2) based on the 6 modeled pressures (dots) and the fitted functions versus the surface atmospheric pressure (dotted lines) for the effective dose calculated based on the water sphere phantom on the martian surface.

tion:

$$D_{surf}(p) = c_D(p) \cdot I_{E_0(p)}, \tag{1}$$

where $D_{surf}(p)$ is the absorbed dose [mGy] on the martain surface under a surface pressure of p, $I_{E_0(p)}$ is the original GLE fluence [particles cm^{-2} MeV^{-1}] at the pivot energy E_0 which is pressure dependent, $c_D(p)$ is the derived coefficient between $I_{E_0(p)}$ and $D_{surf}(p)$ based on all the events studied under a certain surface pressure and has the unit of [mGy cm^2 MeV]. The derived $E_0(p)$ and $c_D(p)$ values are displayed in Figure 7(c) as dots for

6 pressure results. Moreover, we use quadratic functions to fit $E_0(p)$ versus p, and $c_D(p)$ versus p as shown in the legend of the figure so that a continuous coverage of different surface pressures is possible using our empirical function Eq. 1. For any given pressure, $E_0(p)$ and $c_D(p)$ can be implemented in Eq. 1 to quickly derive the surface dose (or dose rate) once the original fluence (or flux) of the SEP event is known.

This approach is also applied to analyze the SEP-induced effective dose for future astronauts on Mars' surface and the following Equation 2 is obtained

$$E_{surf}(p) = c_E(p) \cdot I_{E_0'(p)}. \tag{2}$$

Here, $E_{surf}(p)$ is the body effective dose on martain surface [mSv] under the surface pressure p, $I_{E_0'(p)}$ is the original SEP fluence [particles cm^{-2} MeV^{-1}] at the pivot energy $E_0^{'}$ which is pressure dependent, $c_E(p)$ is the derived coefficient between $I_{E_0'(p)}$ and $E_{surf}(p)$ based on all the events studied under a certain surface pressure p and has the unit of [mSv cm^2 MeV]. The derived $E_0^{'}(p)$ and $c_E(p)$ values are displayed in Figure 7(d). Again, we use quadratic functions to fit $E_0^{'}(p)$ versus p, and $c_E(p)$ versus p as shown in the legend so that the prediction can be made for any given surface pressure between 82 Pa and 1200 Pa.

For future applications, with the derived $c_D(p)$, $c_E(p)$, $E_0(p)$ and $E_0^{'}(p)$ values shown in Figure 7(c) and 7(d) applied to Equations 1 and 2, we can quickly quantify the absorbed dose and effective dose at various locations with different surface pressure p based solely on the SEP fluence at these pivot energies. This can serve as a timely forecast for the global Martian radiation environment.

4 Summary and Conclusion

In order to understand the impact of extreme SEP events on the Martian radiation enrichment at a global scale (different altitude or different locations) , we established a martian radiation model to study the SEP-induced radiation on Mars and its dependence on the atmospheric depths. We considered 6 scenarios of martian atmosphere with surface pressures ranging from 82 Pa at the top of Olympus Mons to 1200 Pa at Hellas Planitia through the state-of-the-art GEANT4 and AtRIS codes and simulated the radiation induced by the 67 SEP spectra which are converted from historical GLE spectra at Earth as shown in Figure 1.

We showed the modification of the proton spectra as SEPs arrive at different Martian locations with different atmospheric depths and derived the induced absorbed dose due to protons under different surface pressures as in Figure 2. We demonstrate that the energy range of protons, which cover 90% of the total proton-induced dose shifts to higher energies as the atmosphere becomes thicker due to the reduction of the proton flux at lower energies being more efficient.

We further derived the absorbed dose in a 300-μm-thick silicon slab, as well as the absorbed dose, dose equivalent, and effective dose calculated based on a 15-cm-radius water sphere phantom above and beneath the martian surface (from the altitude of 70 km in the atmosphere down to the depth of 10 m beneath the surface) with GLE73 on 2021-10-28 as an exampled event shown in Figure 3. The SEP-induced radiation is significantly affected by the martian atmosphere: increase of surface pressure from 82 Pa to 1200 Pa may reduce the surface radiation by an order of magnitude. The result also shows that the Martian soil can more efficiently reduce the SEP impact: at 1 m depth beneath surface, radiation (quantified as absorbed dose, dose equivalent and effective dose) is reduced down to only one percent of that on the surface. Note that the martian soil used in the current model is rather "dry" without content of hydrogen. If consider the soil contains water (with hydrogen atoms) we may expect an enhanced modulation of the secondary fast neutrons (below $\sim$ 10 MeV) as modeled by Röstel et al. (2020). As

a result, the corresponding dose equivalent and effective dose could be lower for such "wet" Martian regolith due to the large biological weighing factor of neutrons around this every range. However, the absorbed dose does not change much as the soil content changes.

The prediction of our model for GLE73 in the silicon slab under a surface pressure of about 753 Pa is 120 µGy which is about 45% smaller than the surface measurement of RAD (216 µGy under a pressure of 742 Pa) in its silicon detector (Guo et al., 2023). This difference is likely due to the fact that the factor $(1/1.5^2)$ that converts the GLE73 spectrum at Earth to Mars is only a general and statistically-averaged assumption which may not be accurate for individual events. In the case of this event, this factor might lead to an underestimation of the actual SEP flux at Mars as discussed in detail in Guo et al. (2023).

Comparing the results of different SEP events, we found that the shielding effect of the martian atmosphere is more effective for softer GLE spectra which have a larger relative contribution of low-energy particles as shown in Figure 4. This highlights the importance of better understanding the SEP spectra properties in order to predict the surface radiation environment and develop shielding strategies.

Finally, we derived the pivot energy and the correlation for the surface absorbed dose and effective dose calculated based on the water sphere phantom following the method of Guo, Wimmer-Schweingruber, et al. (2019) and further explored how the pivot energy and the correlation may differ at different martian locations with different atmospheric pressures. With the derived equations 1 and 2 and the pressure-dependent parameters, we can quickly obtain the radiation doses caused by SEPs solely based on the fluence at the pivot energy without running the global Mars radiation model for complicated calculations.

Therefore, continuous observations monitoring the energetic particles arriving at Mars would be of great benefit for future accurate forecast of the SEP-induced radiation on Mars. Currently, the Mars Energetic Particle Analyzer (MEPA, Tang et al., 2020) on board the first Chinese Mars exploration mission (Tianwen-1) has been monitoring the flux of particles with energy between 2 and 100 MeV at Mars orbit since February 2021. This energy range compensates that by the SEP instrument of Mars Atmosphere and Volatile EvolutioN (MAVEN, Larson et al., 2015) orbiter which measures the flux of particles with energy lower than about 6 MeV. However, the pivot energies we derived vary from $\sim$ 100 MeV ($E_0^{'}$ for 82 Pa) to $\sim$ 350 MeV (E_0 for 1200 Pa) which are mostly beyond the current energy range covered by the existing instruments. Carrying a particle detector with a higher energy range can be considered in future Mars exploration missions. Besides, SEP modeling approaches that predict SEP fluxes at energies of 100s of MeV and towards the direction of Mars will be of great importance for mitigating future Martian radiation hazards induced by extreme SEPs (e.g., Whitman et al., 2022).

Acknowledgments

We acknowledge the support by the Strategic Priority Program of the Chinese Academy of Sciences (Grant No. XDB41000000), the National Natural Science Foundation of China (Grant No. 42074222, 42188101) and the CNSA pre-research Project on Civil Aerospace Technologies (Grant No. D020104). Part of this work used computational and storage services associated with the Hoffman2 Shared Cluster provided by UCLA Institute for Digital Research and Education's Research Technology Group.

Open Research

The AtRIS code used in this study is uploaded at Zenodo platform (under the DOI code https://doi.org/10.5281/zenodo.3633451). The installation and implementation in-

structions are further detailed (at this page: `https://et-wiki.physik.uni-kiel.de/atris/atris`).

References

Agostinelli, S., Allison, J., Amako, K., Apostolakis, J., Araujo, H., Arce, P., ... others (2003). GEANT4: a simulation toolkit. *Nuclear Instruments and Methods in Physics Research Section A*, *506*(3), 250–303.

Band, D., Matteson, J., Ford, L., Schaefer, B., Palmer, D., Teegarden, B., ... others (1993). Batse observations of gamma-ray burst spectra. i-spectral diversity. *The Astrophysical Journal*, *413*, 281–292.

Banjac, S., Herbst, K., & Heber, B. (2018). The atmospheric radiation interaction simulator (AtRIS) - description and validation. *Journal of Geophysical Research: Space Physics*, *123*(ja). doi: 10.1029/2018JA026042

Bruno, A., Christian, E., De Nolfo, G., Richardson, I. G., & Ryan, J. (2019). Spectral analysis of the september 2017 solar energetic particle events. *Space Weather*, *17*(3), 419–437.

Bryant, D. A., Cline, T. L., Desai, U. D., & McDonald, F. B. (1962). Explorer 12 observations of solar cosmic rays and energetic storm particles after the solar flare of september 28, 1961. *Journal of Geophysical Research (1896-1977)*, *67*(13), 4983-5000. Retrieved from `https://agupubs.onlinelibrary.wiley.com/doi/abs/10.1029/JZ067i013p04983` doi: https://doi.org/10.1029/JZ067i013p04983

Cucinotta, F. A., Kim, M.-H. Y., Chappell, L. J., & Huff, J. L. (2013). How safe is safe enough? radiation risk for a human mission to Mars. *PLoS One*, *8*(10), e74988. doi: 10.1371/journal.pone.0074988

Da Pieve, F., Gronoff, G., Guo, J., Mertens, C., Neary, L., Gu, B., ... Cleri, F. (2021). Radiation environment and doses on mars at oxia planum and mawrth vallis: Support for exploration at sites with high biosignature preservation potential. *Journal of Geophysical Research: Planets*, *126*(1), e2020JE006488.

Dobynde, M., Shprits, Y., Drozdov, A. Y., Hoffman, J., & Li, J. (2021). Beating 1 sievert: Optimal radiation shielding of astronauts on a mission to mars. *Space Weather*, *19*(9), e2021SW002749.

Ehresmann, B., Burmeister, S., Wimmer-Schweingruber, R. F., & Reitz, G. (2011). Influence of higher atmospheric pressure on the martian radiation environment: Implications for possible habitability in the noachian epoch. *Journal of Geophysical Research : Space physics*, *116*(A15), 10106. doi: 10.1029/2011JA016616

Forget, F., Hourdin, F., Fournier, R., Hourdin, C., Talagrand, O., Collins, M., ... Huot, J.-P. (1999, October). Improved general circulation models of the Martian atmosphere from the surface to above 80 km. *Journal of Geophysical Research: Planets*, *104*(E10), 24155-24176. doi: 10.1029/1999JE001025

Guo, J., Banjac, S., Röstel, L., Terasa, J. C., Herbst, K., Heber, B., & Wimmer-Schweingruber, R. F. (2019). Implementation and validation of the GEANT4/AtRIS code to model the radiation environment at Mars. *Journal of Space Weather and Space Climate*, *9*(A2). doi: 10.1051/swsc/2018051

Guo, J., Li, X., Zhang, J., Dobynde, M. I., Wang, Y., Xu, Z., ... Zhuang, B. (2023). The first ground level enhancement seen on three planetary surfaces: Earth, moon and mars. *Geophysical Research Letters*.

Guo, J., Slaba, C., Tony C.and Zeitlin, Wimmer-Schweingruber, R. F., Badavi, F. F., Böhm, E., Böttcher, S., ... Rafkin, S. (2017). Dependence of the martian radiation environment on atmospheric depth: modelling and measurement. *Journal of Geophysical Research: Planets*, *122*(2), 329–341. (2016JE005206) doi: 10.1002/2016JE005206

Guo, J., Wimmer-Schweingruber, R. F., Wang, Y., Grande, M., Matthiä, D., Zeitlin,

C., ... Hassler, D. M. (2019). The pivot energy of solar energetic particles affecting the martian surface radiation environment. *The Astrophysical Journal Letters*, *883*(1), L12. doi: 10.3847/2041-8213/ab3ec2

Guo, J., Zeitlin, C., Wimmer-Schweingruber, R. F., Hassler, D. M., Ehresmann, B., Rafkin, S., ... Wang, Y. (2021). Radiation environment for future human exploration on the surface of mars: the current understanding based on msl/rad dose measurements. *The Astronomy and Astrophysics Review*, *29*(1), 1–81.

Hassler, D. M., Zeitlin, C., Wimmer-Schweingruber, R. F., Böttcher, S. I., Martin, C., Andrews, J., ... others (2012). The Radiation Assessment Detector (RAD) investigation. *Space Science Reviews*, *170*(1), 503–558. doi: 10.1007/s11214-012-9913-1

Hassler, D. M., Zeitlin, C., Wimmer-Schweingruber, R. F., Ehresmann, B., Rafkin, S., Eigenbrode, J. L., ... others (2014). Mars's surface radiation environment measured with the Mars Science Laboratory's curiosity rover. *Science*, *343*(6169), 1244797. doi: 10.1126/science.1244797

ICRP. (1992, Feb). Recommendations of the international commission on radiological protection (icrp) 1990. *European Journal of Nuclear Medicine*, *19*(2), 77-79. Retrieved from `https://doi.org/10.1007/BF00184120` doi: 10.1007/BF00184120

ICRP. (2007). The icrp 2007 recommendations. *Radiation protection dosimetry*, *127*(1-4), 2–7. doi: 10.1093/rpd/ncm246

ICRP. (2013). Icrp publication 123: Assessment of radiation exposure of astronauts in space. *Annals of the ICRP*, *42*(4), 1–339. doi: 10.1016/j.icrp.2013.05.004

Lario, D., Aran, A., Gómez-Herrero, R., Dresing, N., Heber, B., Ho, G., ... Roelof, E. (2013). Longitudinal and radial dependence of solar energetic particle peak intensities: Stereo, ace, soho, goes, and messenger observations. *The Astrophysical Journal*, *767*(1), 41. doi: 10.1088/0004-637X/767/1/41

Larson, D. E., Lillis, R. J., Lee, C. O., Dunn, P. A., Hatch, K., Robinson, M., ... others (2015). The maven solar energetic particle investigation. *Space Science Reviews*, *195*(1-4), 153–172.

Martucci, M., Laurenza, M., Benella, S., Berrilli, F., Del Moro, D., Giovannelli, L., ... Zuccon, P. (2023). The first ground-level enhancement of solar cycle 25 as seen by the high-energy particle detector (hepd-01) on board the cses-01 satellite. *Space Weather*, *21*(1), e2022SW003191. Retrieved from `https://agupubs.onlinelibrary.wiley.com/doi/abs/10.1029/2022SW003191` (e2022SW003191 2022SW003191) doi: https://doi.org/10.1029/2022SW003191

Matthiä, D., Berger, T., & Reitz, G. (2013). Organ shielding and doses in Low-Earth orbit calculated for spherical and anthropomorphic phantoms. *Advances in Space Research*, *52*(3), 528–535. doi: 10.1016/j.asr.2013.03.025

Miroshnichenko, L., Vashenyuk, E., & Pérez-Peraza, J. (2013). Solar cosmic rays: 70 years of ground-based observations. *Geomagnetism and Aeronomy*, *53*(5), 541–560. doi: 10.1134/S0016793213050125

O'Neill, P., Golge, S., & Slaba, T. (2015). Badhwar–O'Neill 2014 galactic cosmic ray flux model. *NASA Technical Report*, *218569*. Retrieved from `https://ntrs.nasa.gov/archive/nasa/casi.ntrs.nasa.gov/20150003026.pdf`

Raukunen, O., Vainio, R., Tylka, A. J., Dietrich, W. F., Jiggens, P., Heynderickx, D., ... Siipola, R. (2018). Two solar proton fluence models based on ground level enhancement observations. *J. Space Weather Space Clim.*, *8*, A04. Retrieved from `https://doi.org/10.1051/swsc/2017031` doi: 10.1051/swsc/2017031

Röstel, L., Guo, J., Banjac, S., Wimmer-Schweingruber, R. F., & Heber, B. (2020). Subsurface radiation environment of Mars and its implication for shielding protection of future habitats. *Journal of Geophysical Research: Planets*, *125*(3), e2019JE006246. doi: 10.1029/2019JE006246

Saganti, P. B., Cucinotta, F. A., Wilson, J. W., Simonsen, L. C., & Zeitlin, C. (2004). Radiation climate map for analyzing risks to astronauts on the Mars surface from galactic cosmic rays. *Space Science Reviews*, *110*(1-2), 143–156. doi: 10.1007/978-0-306-48600-5_5

Tang, S., Wang, Y., Zhao, H., Fang, F., Qian, Y., Zhang, Y., ... others (2020). Calibration of Mars Energetic Particle Analyzer (MEPA). *Earth and Planetary Physics*, *4*(4), 355–363. doi: 10.26464/epp2020055

Tylka, A. J., & Dietrich, W. F. (2009). A new and comprehensive analysis of proton spectra in ground-level enhanced (gle) solar particle events..

Whitman, K., Egeland, R., Richardson, I. G., Allison, C., Quinn, P., Barzilla, J., ... Hosseinzadeh, P. (2022). Review of solar energetic particle models. *Advances in Space Research*. Retrieved from `https://www.sciencedirect.com/science/article/pii/S0273117722007244` doi: https://doi.org/10.1016/j.asr.2022.08.006

Zeitlin, C., Hassler, D. M., Cucinotta, F. A., Ehresmann, B., Wimmer-Schweingruber, R. F., Brinza, D. E., ... Reitz, G. (2013). Measurements of energetic particle radiation in transit to Mars on the Mars Science Laboratory. *Science*, *340*(6136), 1080–1084. Retrieved from `http://science.sciencemag.org/content/340/6136/1080` doi: 10.1126/science.1235989

Zhang, J., Guo, J., Dobynde, M. I., Wang, Y., & Wimmer-Schweingruber, R. F. (2022). From the top of martian olympus to deep craters and beneath: Mars radiation environment under different atmospheric and regolith depths. *Journal of Geophysical Research: Planets*, *127*(3), e2021JE007157. doi: 10.1029/2021JE007157

Figure 1.

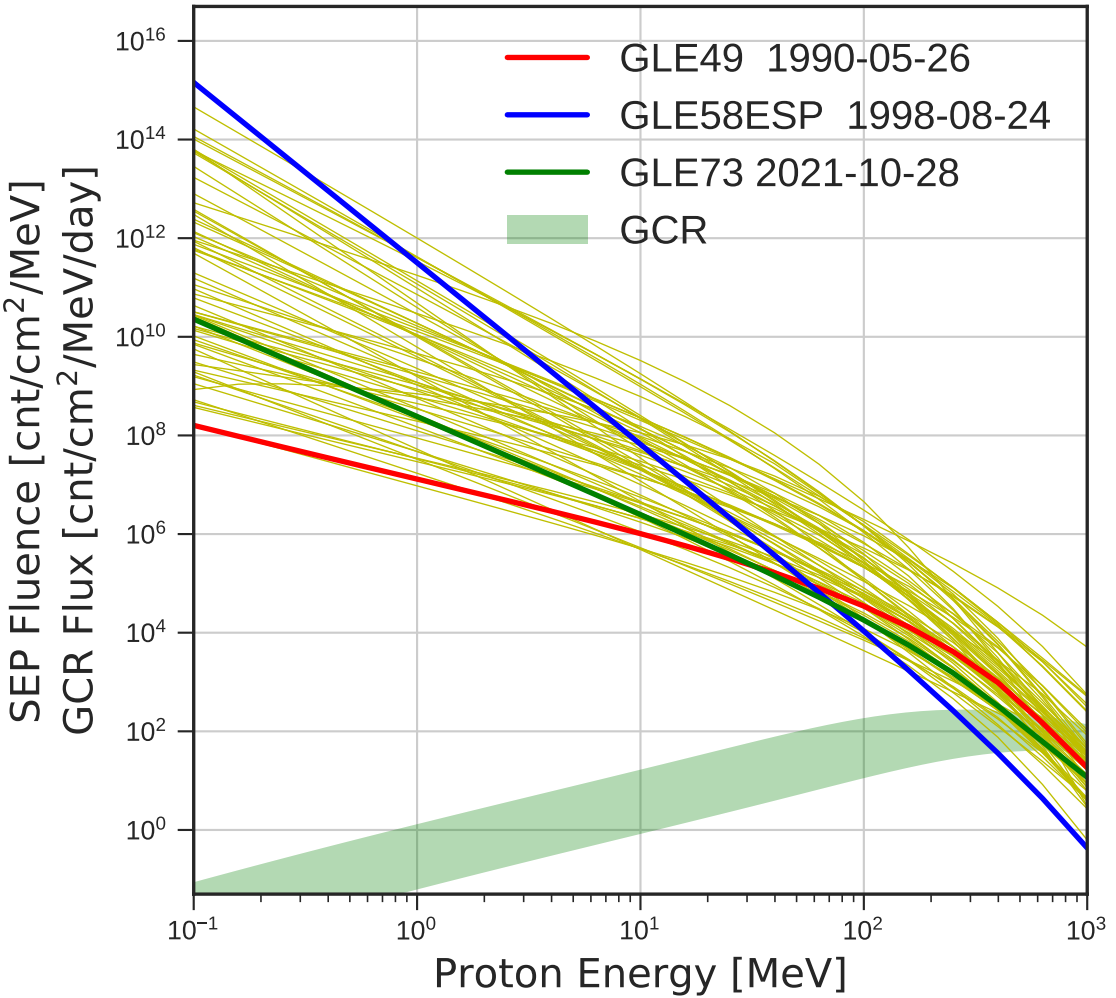
GLE49 1990-05-26
GLE58ESP 1998-08-24
GLE73 2021-10-28
GCR
SEP Fluence [cnt/cm^2/MeV]
GCR Flux [cnt/cm^2/MeV/day]
10^{16}
10^{14}
10^{12}
10^{10}
10^{8}
10^{6}
10^{4}
10^{2}
10^{0}
10^{-1}
10^{0}
10^{1}
10^{2}
10^{3}
Proton Energy [MeV]

Figure 2a.

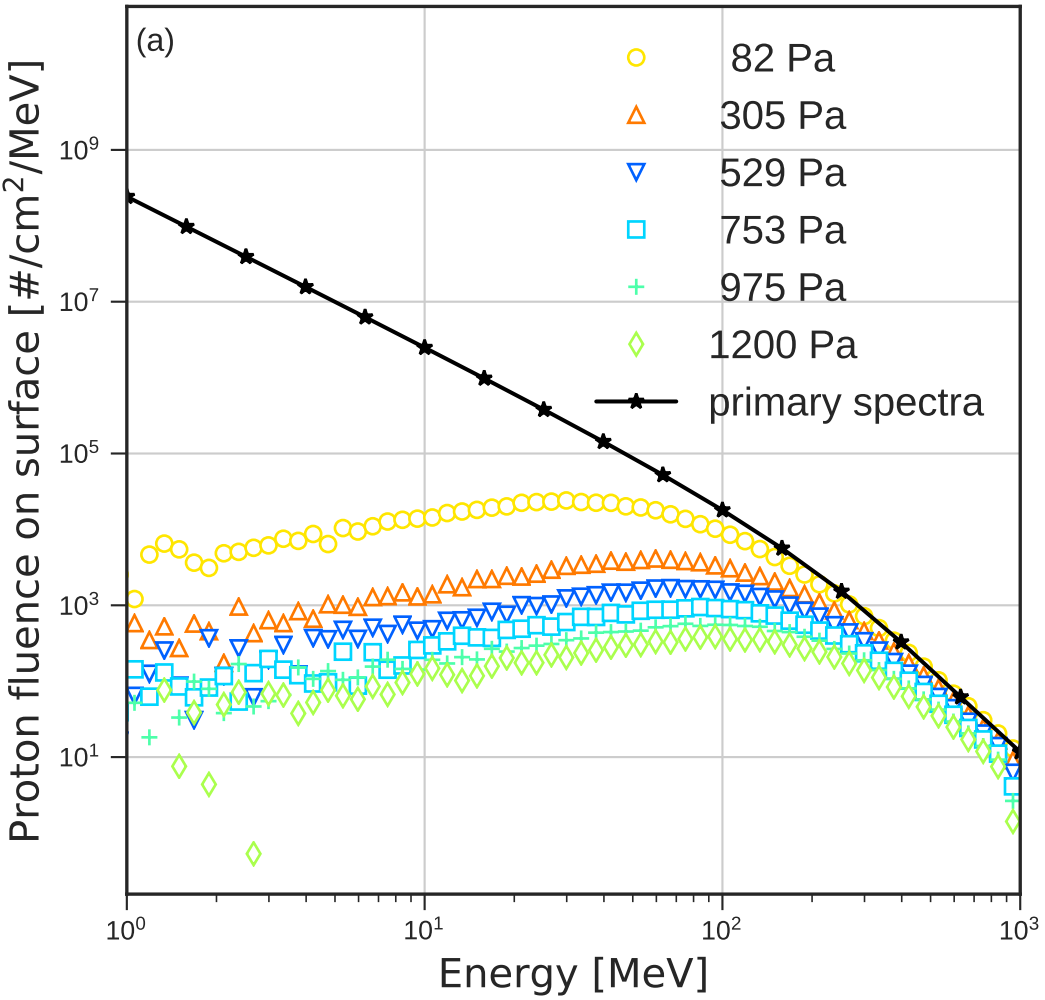
(a)
82 Pa
305 Pa
529 Pa
753 Pa
975 Pa
1200 Pa
primary spectra
Proton fluence on surface [#/cm^2/MeV]
10^9
10^7
10^5
10^3
10^1
10^0
10^1
10^2
10^3
Energy [MeV]

Figure 2bc.

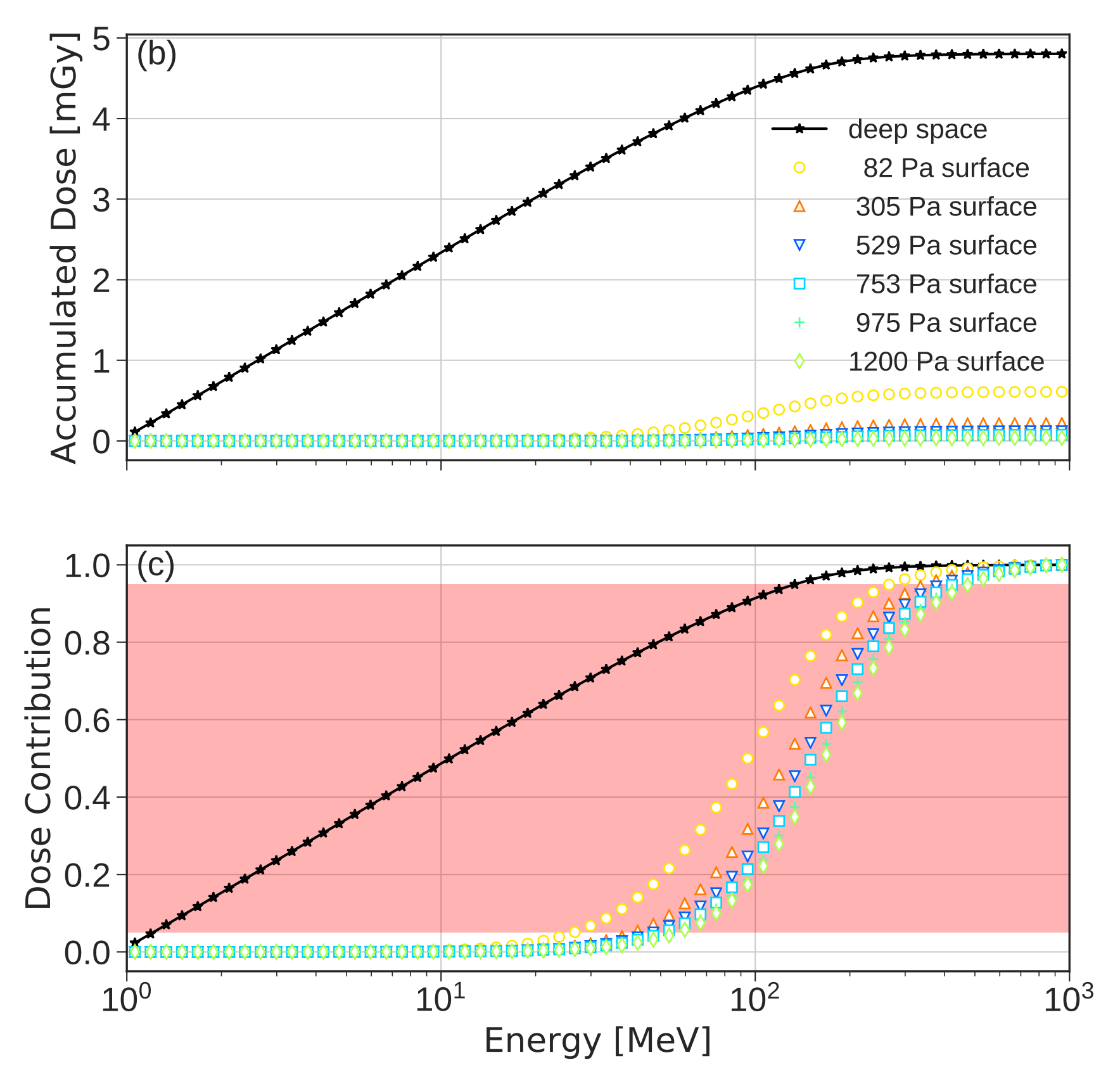
(b)
Accumulated Dose [mGy]
0
1
2
3
4
5
deep space
82 Pa surface
305 Pa surface
529 Pa surface
753 Pa surface
975 Pa surface
1200 Pa surface
(c)
Dose Contribution
0.0
0.2
0.4
0.6
0.8
1.0
10^0
10^1
10^2
10^3
Energy [MeV]

Figure 3a.

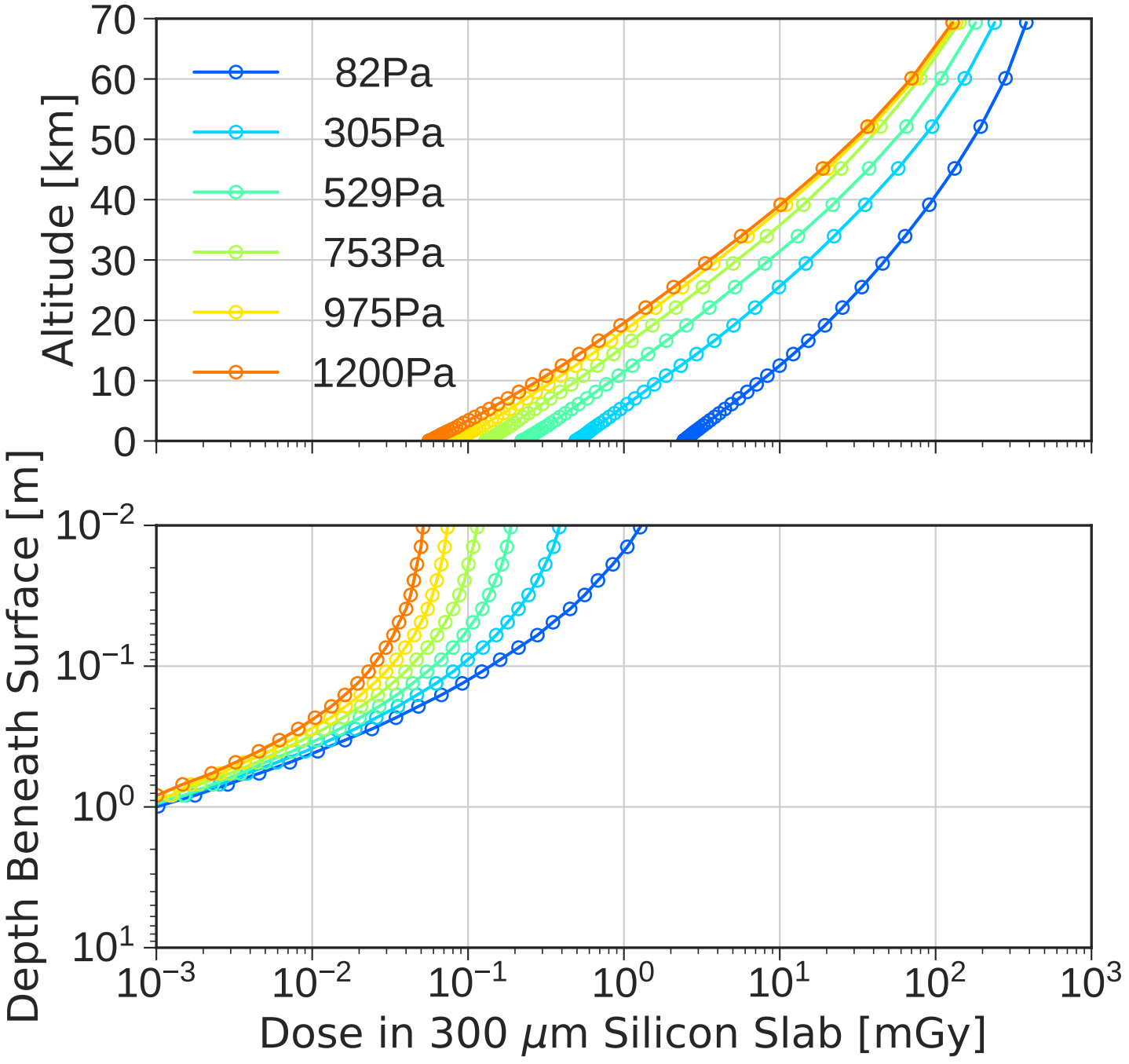
82Pa
305Pa
529Pa
753Pa
975Pa
1200Pa
Altitude [km]
0
10
20
30
40
50
60
70
Depth Beneath Surface [m]
10^{-2}
10^{-1}
10^{0}
10^{1}
10^{-3}
10^{-2}
10^{-1}
10^{0}
10^{1}
10^{2}
10^{3}
Dose in 300 μm Silicon Slab [mGy]

Figure 3b.

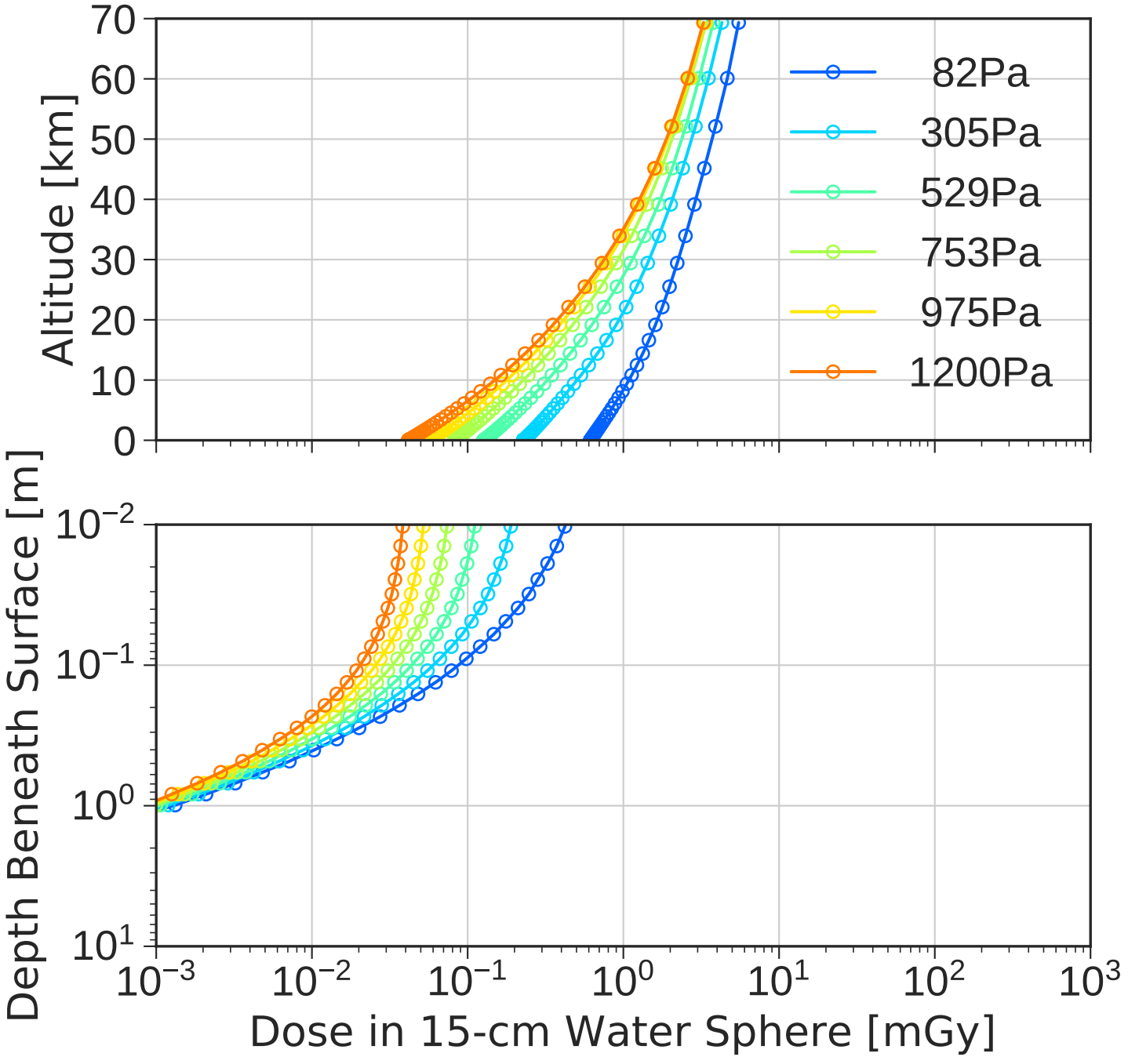
Altitude [km]
70
60
50
40
30
20
10
0
82Pa
305Pa
529Pa
753Pa
975Pa
1200Pa
Depth Beneath Surface [m]
10^{-2}
10^{-1}
10^{0}
10^{1}
10^{-3}
10^{-2}
10^{-1}
10^{0}
10^{1}
10^{2}
10^{3}
Dose in 15-cm Water Sphere [mGy]

Figure 3c.

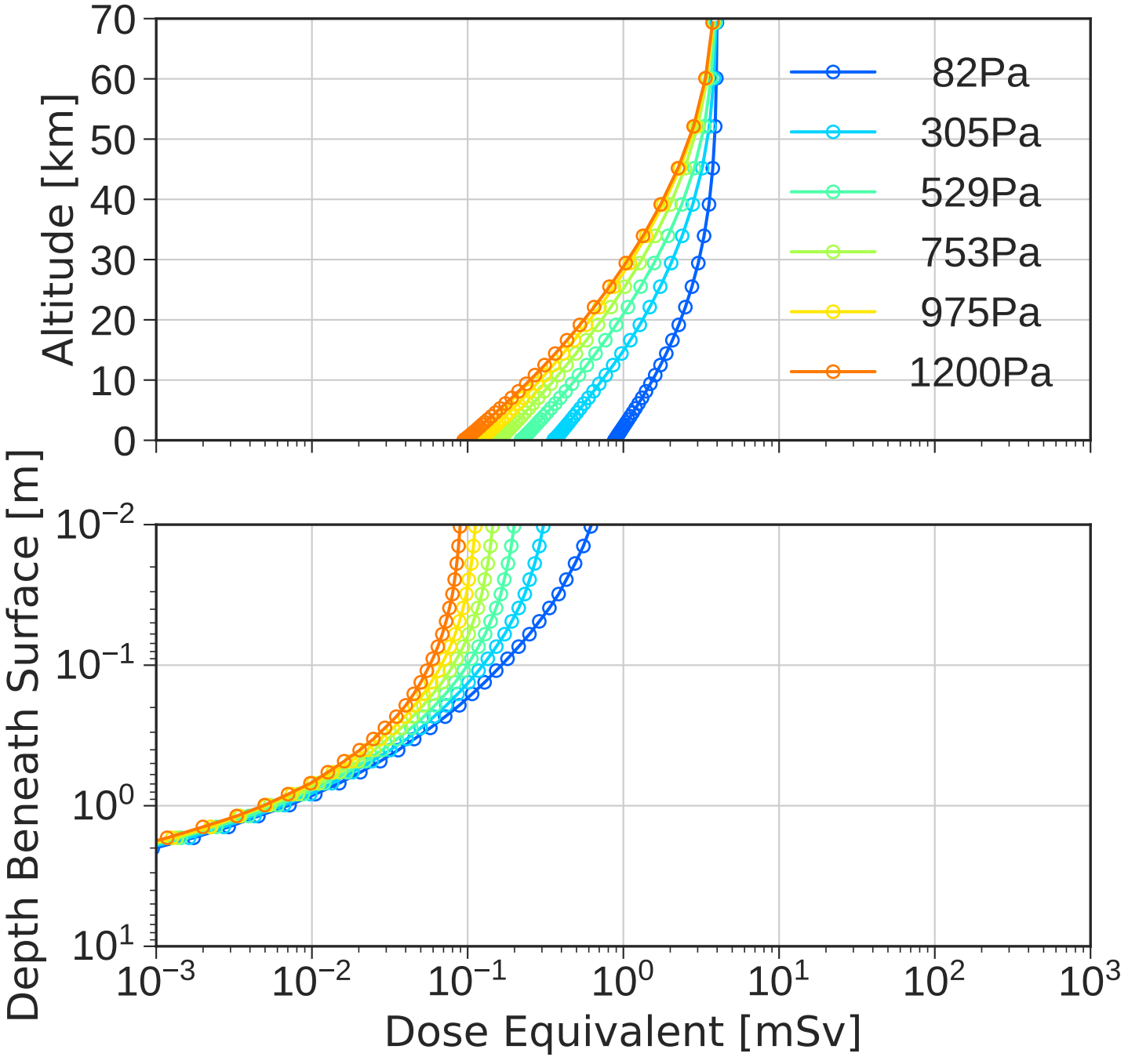
Altitude [km]
70
60
50
40
30
20
10
0
82Pa
305Pa
529Pa
753Pa
975Pa
1200Pa
Depth Beneath Surface [m]
10^{-2}
10^{-1}
10^{0}
10^{1}
10^{-3}
10^{-2}
10^{-1}
10^{0}
10^{1}
10^{2}
10^{3}
Dose Equivalent [mSv]

Figure 3d.

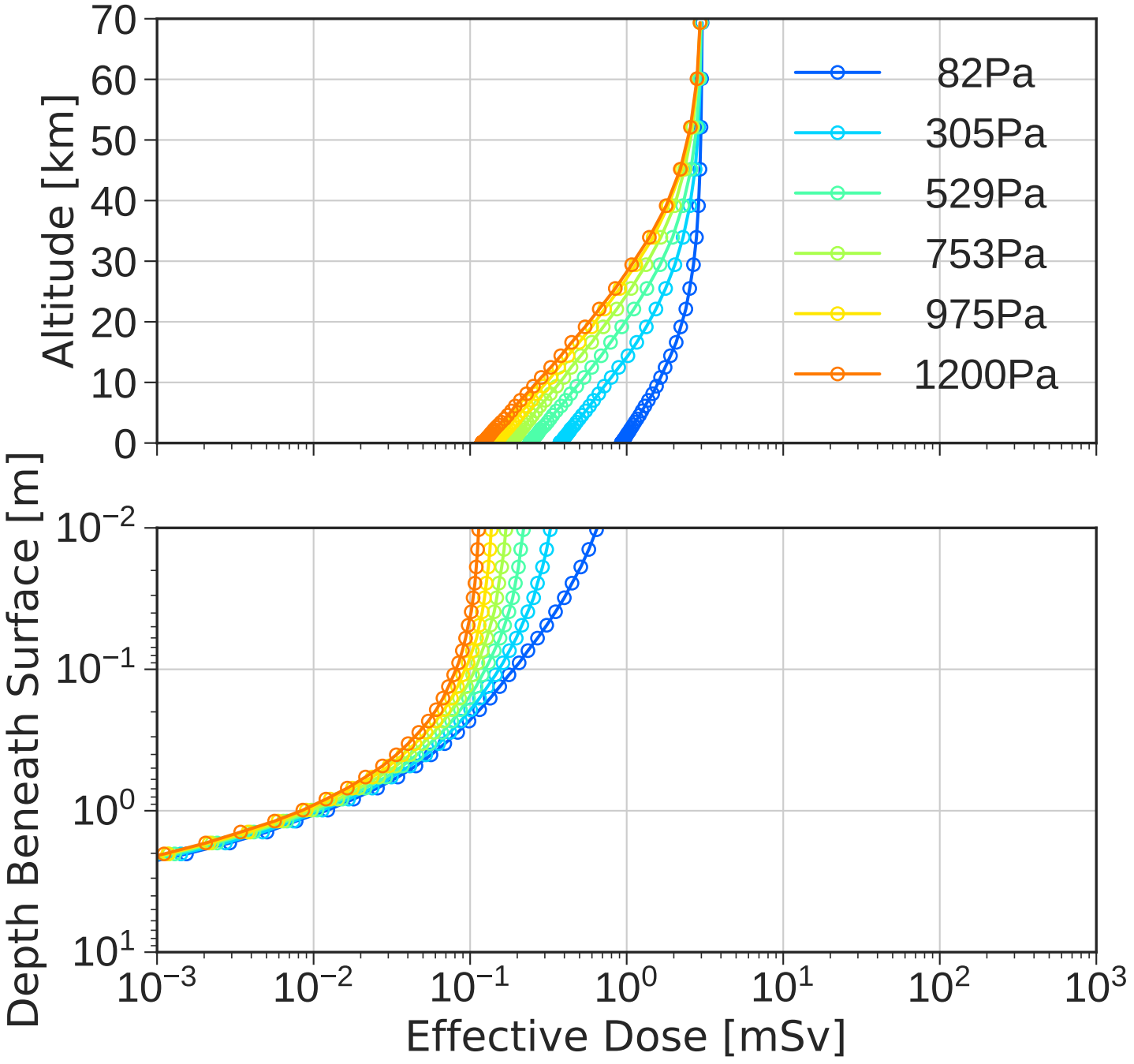
Altitude [km]
70
60
50
40
30
20
10
0
82Pa
305Pa
529Pa
753Pa
975Pa
1200Pa
Depth Beneath Surface [m]
10^{-2}
10^{-1}
10^{0}
10^{1}
10^{-3}
10^{-2}
10^{-1}
10^{0}
10^{1}
10^{2}
10^{3}
Effective Dose [mSv]

Figure 4a.

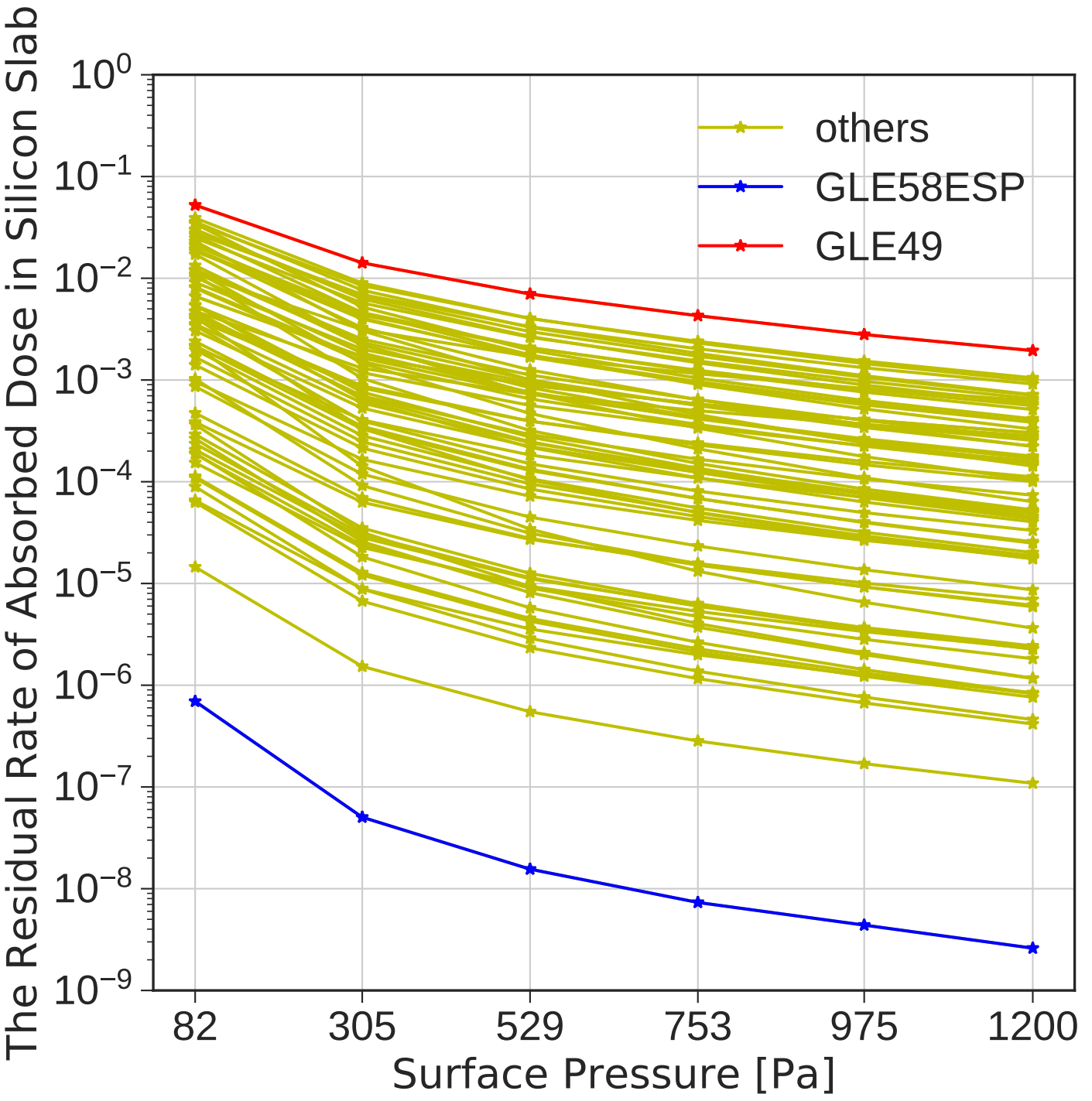
The Residual Rate of Absorbed Dose in Silicon Slab
10^{0}
10^{-1}
10^{-2}
10^{-3}
10^{-4}
10^{-5}
10^{-6}
10^{-7}
10^{-8}
10^{-9}
others
GLE58ESP
GLE49
82
305
529
753
975
1200
Surface Pressure [Pa]

Figure 4b.

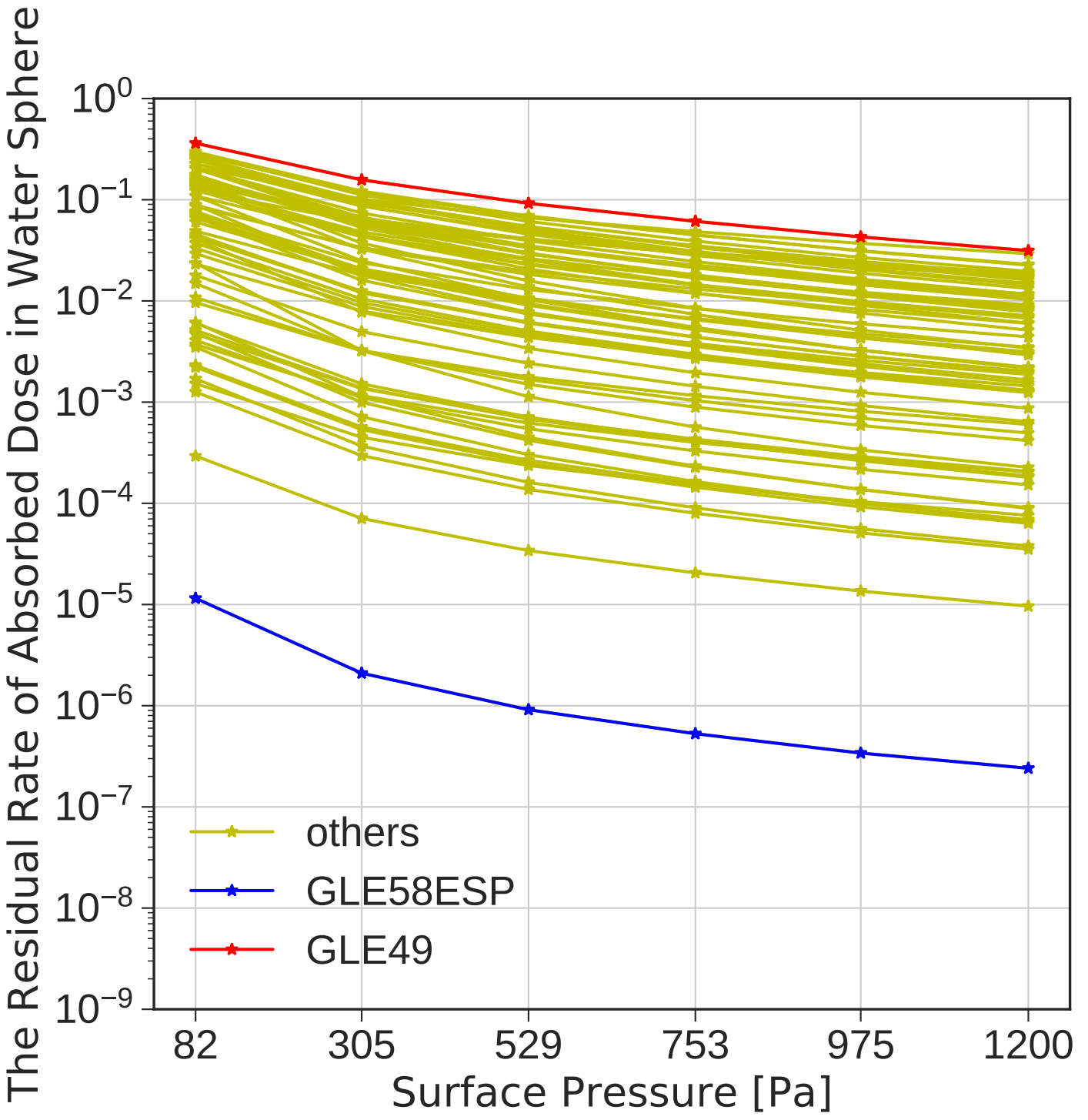
The Residual Rate of Absorbed Dose in Water Sphere
10^{0}
10^{-1}
10^{-2}
10^{-3}
10^{-4}
10^{-5}
10^{-6}
10^{-7}
10^{-8}
10^{-9}
82
305
529
753
975
1200
Surface Pressure [Pa]
others
GLE58ESP
GLE49

Figure 5.

Absorbed Dose in Water Sphere on Martian Surface [mGy]

10^{3}
10^{2}
10^{1}
10^{0}
10^{-1}
10^{-2}

1200 Pa
975 Pa
753 Pa
529 Pa
305 Pa
82 Pa

5 7 8 9 10 11 12 13 16 19 21 22 23 24 25 26 27 28 29 30 31 32 35 36 37 38 39 40 41 42 42ESP 43 43ESP 44 45 46 47 48 49 50 51 52 53 54 55 56 57 58 58ESP 59 59ESP 60 61 62 62ESP 63 64 65 65ESP 66 67 68 69 70 71 72 73

GLE

Figure 6.

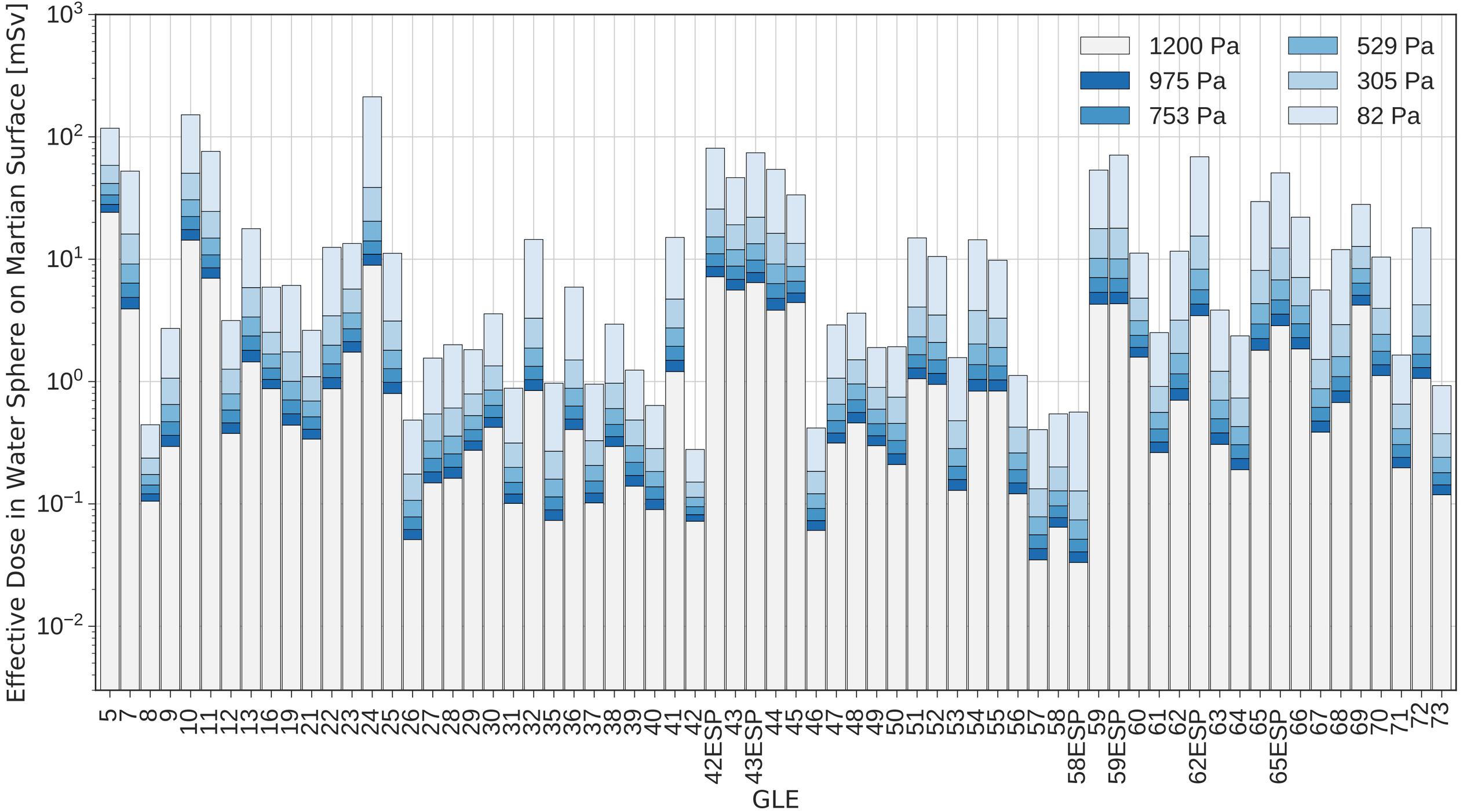
Effective Dose in Water Sphere on Martian Surface [mSv]
10^3
10^2
10^1
10^0
10^{-1}
10^{-2}
1200 Pa
975 Pa
753 Pa
529 Pa
305 Pa
82 Pa
5 7 8 9 10 11 12 13 16 19 21 22 23 24 25 26 27 28 29 30 31 32 35 36 37 38 39 40 41 42 42ESP 43 43ESP 44 45 46 47 48 49 50 51 52 53 54 55 56 57 58 58ESP 59 59ESP 60 61 62 62ESP 63 64 65 65ESP 66 67 68 69 70 71 72 73
GLE

Figure 7a.

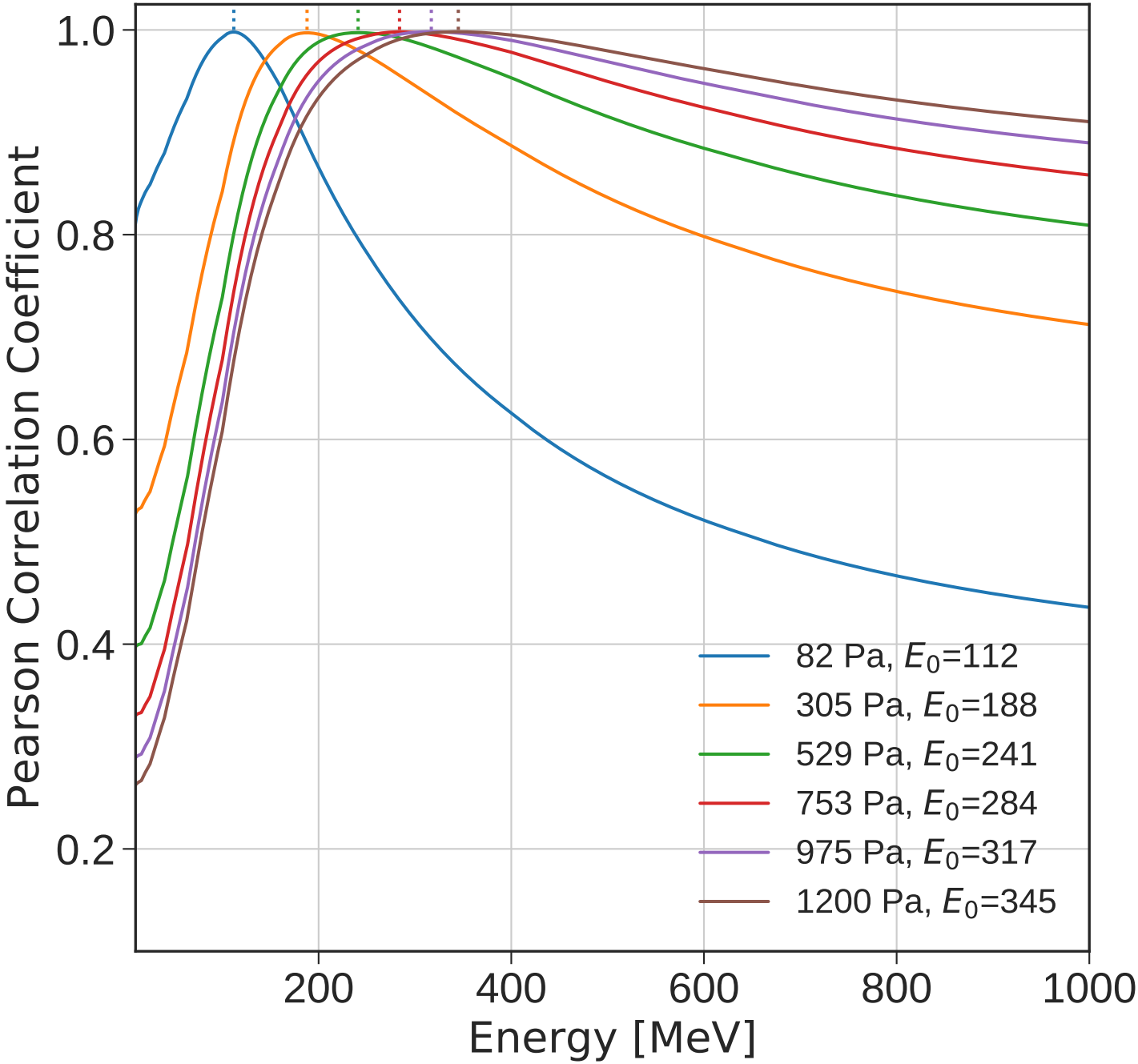
1.0
0.8
0.6
0.4
0.2
Pearson Correlation Coefficient
200
400
600
800
1000
Energy [MeV]
82 Pa, E_0=112
305 Pa, E_0=188
529 Pa, E_0=241
753 Pa, E_0=284
975 Pa, E_0=317
1200 Pa, E_0=345

Figure 7b.

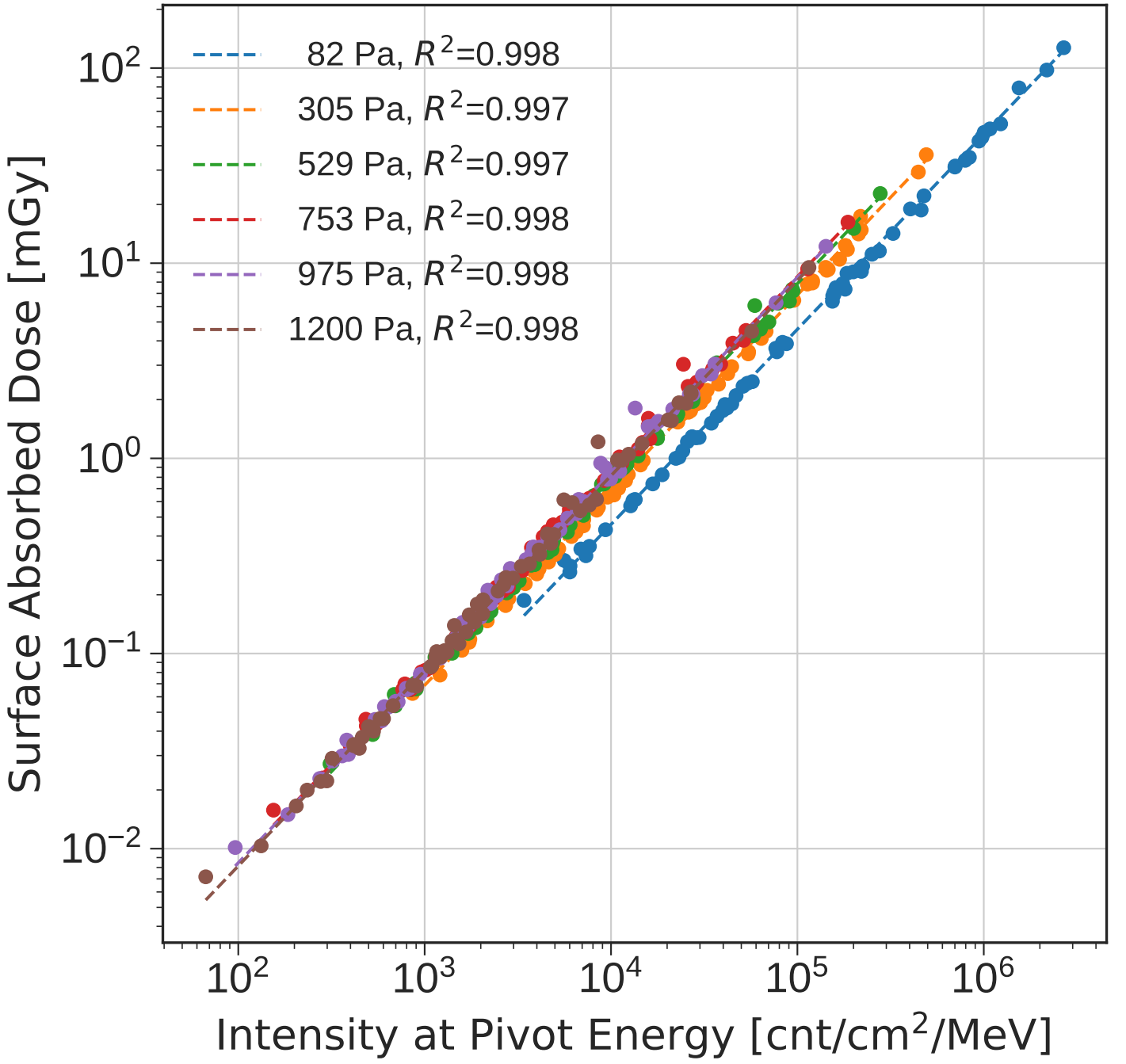
82 Pa, R^2=0.998
305 Pa, R^2=0.997
529 Pa, R^2=0.997
753 Pa, R^2=0.998
975 Pa, R^2=0.998
1200 Pa, R^2=0.998
Surface Absorbed Dose [mGy]
10^2
10^1
10^0
10^{-1}
10^{-2}
10^2
10^3
10^4
10^5
10^6
Intensity at Pivot Energy [cnt/cm^2/MeV]

Figure 7c.

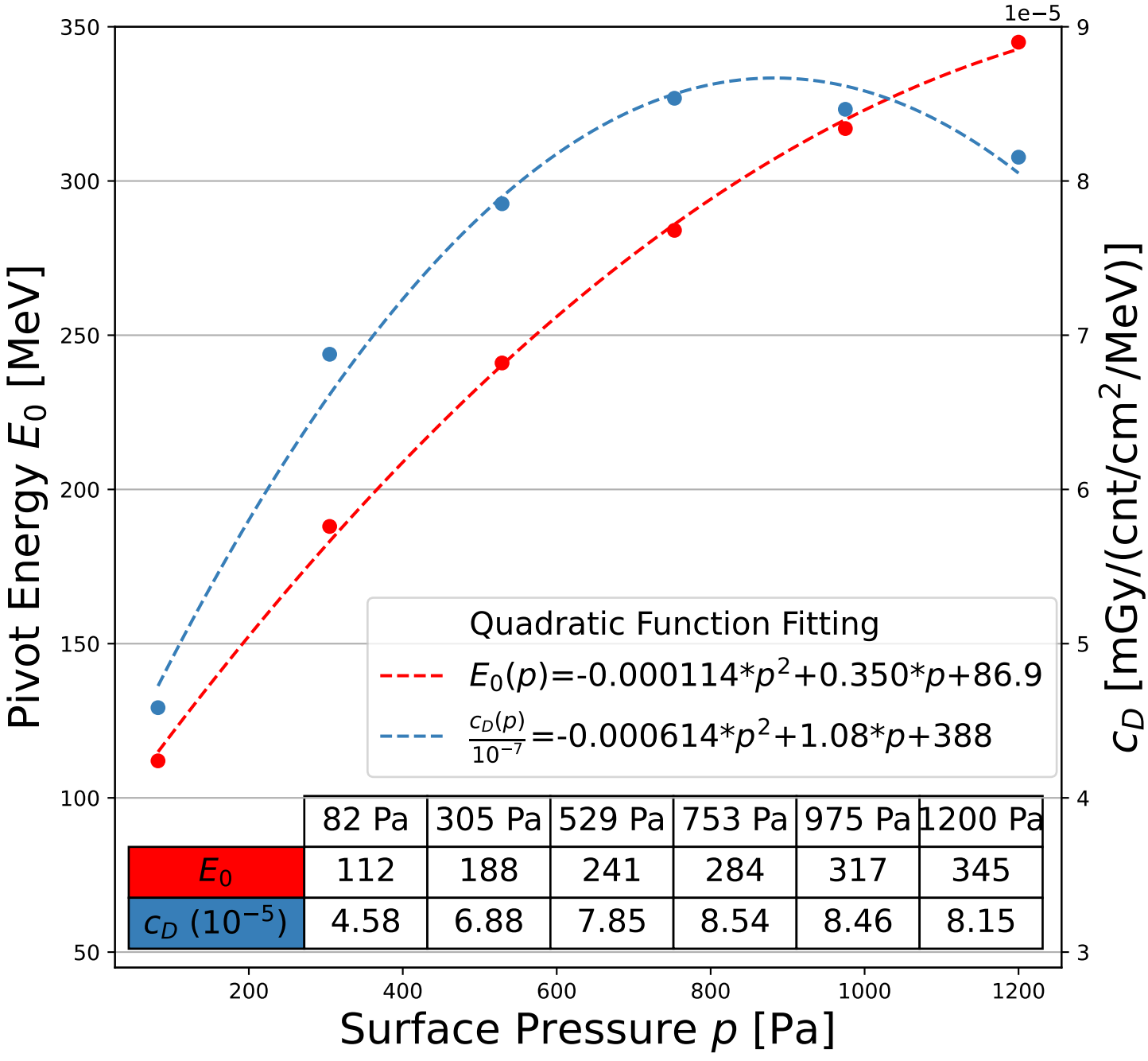

	82 Pa	305 Pa	529 Pa	753 Pa	975 Pa	1200 Pa
E_0	112	188	241	284	317	345
c_D (10^{-5})	4.58	6.88	7.85	8.54	8.46	8.15

Figure 7d.

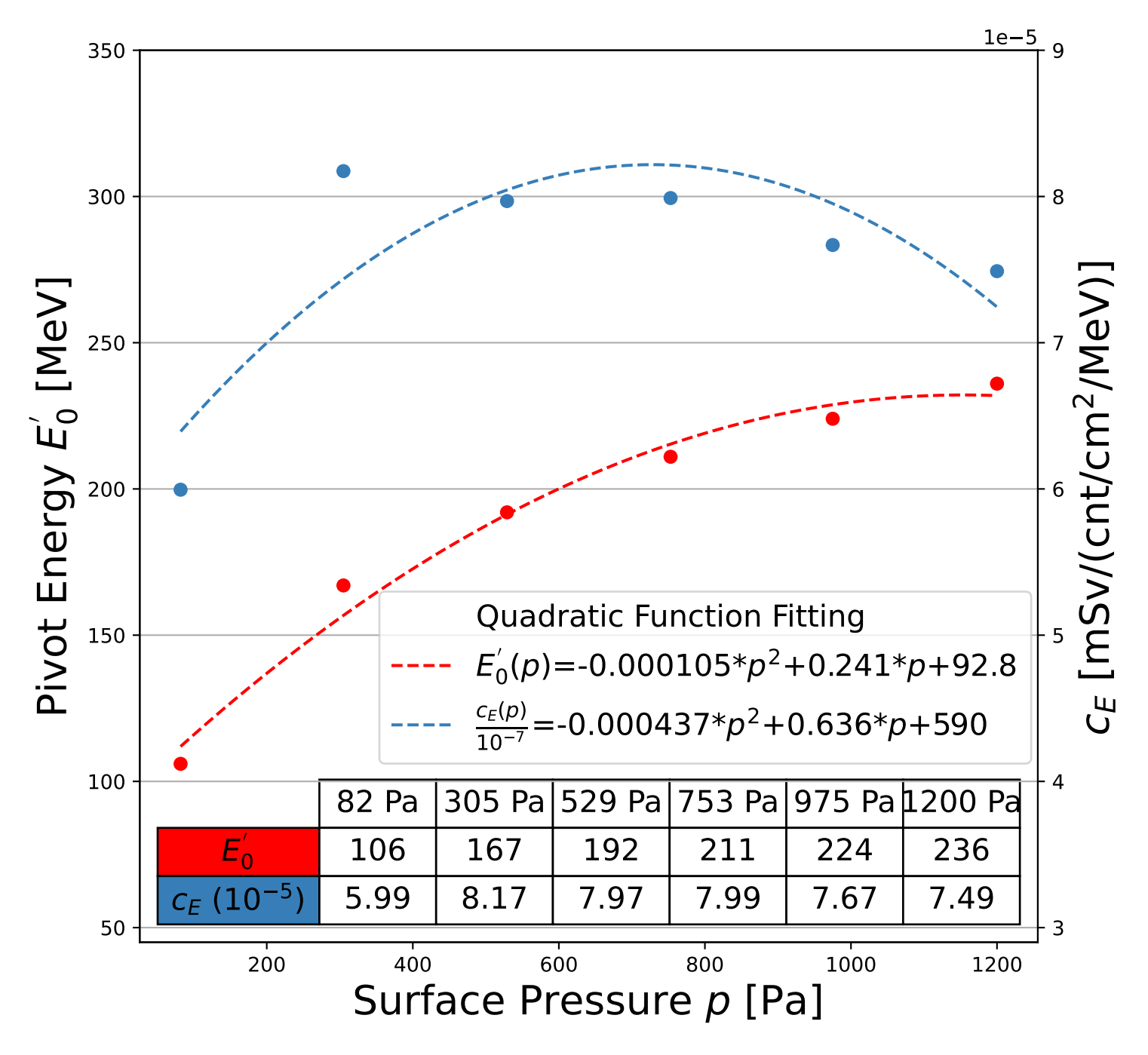

	82 Pa	305 Pa	529 Pa	753 Pa	975 Pa	1200 Pa
$E_0^{'}$	106	167	192	211	224	236
c_E (10^{-5})	5.99	8.17	7.97	7.99	7.67	7.49